The Pennsylvania State University

The Graduate School

College of Engineering

EXPERIMENTAL STUDY OF THE DUST TRAIL PHENOMENON IN A WIND TUNNEL

A Thesis in

Mechanical Engineering

by

Gokhan Akarslan

Submitted in Partial Fulfillment
of the Requirements
for the Degree of

Master of Science

December 2018

The thesis of Gokhan Akarslan was reviewed and approved* by the following:

Rui Ni
Professor of Mechanical Engineering
Thesis Adviser

Bo Cheng
Assistant Professor of Mechanical Engineering

Mary Frecker
Associate Head of Graduate Programs for Mechanical Engineering

*Signatures are on file in the Graduate School.

ABSTRACT

Dust trail behind a moving vehicle is an undesirable situation for human health and military operations. However, very little is known about the dust emission and dust deposition from moving vehicle. Thus, a better understanding is required to eliminate dust dispersion. As an initial step, this work aims to study problem experimentally for scalable, simplified object, in this case, a cylinder. This experimental study was performed in a wind tunnel to observe how dust emission and dust deposition are related to Reynolds number and a gap between the wind tunnel bottom wall and cylinder. Experiments were repeated for various Reynolds numbers and the different gap to cylinder diameter ratios, while the Reynolds numbers which based on the cylinder diameter are in the range of 12655 to 29000, the gap to diameter ratios are between 0.1 and 0.5.

TABLE OF CONTENTS

LIST OF FIGURES

LIST OF TABLES

ACKNOWLEDGEMENTS

I would like to express my deep sense of gratefulness to Dr. Rui Ni not only for being my thesis advisor but also his unlimited support and encouragement in all conditions throughout my studies here at Pennsylvania State University, without his invaluable guidance this could not have been possible. I also am grateful for the environment which he created in the lab, and I could find a chance to know and work together with great team members, Ashwanth Salibindla, Ashik U. M. Masuk, and Morgan Austin under his leadership. I would like to thank Taehoon Kim for his thoughts and help. I would like to express my thanks to Dr. Bo Cheng for his interest in serving as a committee member.

I am thankful to my country, Turkey, and Turkish Petroleum Corporation who provided the opportunity for me to study for my Master's degree at the Pennsylvania State University.

Finally, I would like to express my deepest gratitude to my family and friends for believing in me and supporting me all the time.

Chapter 1

Introduction

1.1 Motivation and Objectives

Most industrial and natural flow processes have a complex multiphase flow where the continuous phase interchanges momentum, mass, energy or heat with a dispersed particle as a solid, gas or liquid phase, in which one of the phases is connected continuously. Some examples of these kinds of flows in nature occur in rain clouds, river or ocean flows with sedimentation and, desert storms. Furthermore, fuel-air mixture in combustion engines, sprays, many petrochemical processes, and fluidized bed reactors are among some of the engineering examples that include of particle-laden flow.

The dust trail behind a car, which stems from vehicle motion, is another solid-gas multiphase flow that is particularly interesting. Dust trail is significant because of two reasons; first, it is detrimental to human health, particularly in regions near to deserts environment, second, in military actions, especially in Middle East zones, dust trail makes troops very detectable even from far away distances. Although there is not a practical solution to this problem, the challenge is uttered in Technical Challenges of the U.S. Army's Ground Combat Vehicle Program to Congressional Budget Office with the words

"No U.S. ground combat system that has been deployed to date has an effective means of preventing dust signatures from forming, especially in dry environments" [1].

Furthermore, as mentioned before, dust is an essential phenomenon for desert-like environments, and the research which covers long-term statistics shows that dust problem has deteriorated over decades and desertification process is accelerating because of climate change [2]. This escalating problem causes more dust emission on unpaved roads due to vehicle motions.

Despite these issues, our knowledge about how dust is emitted and dispersed behind moving vehicles is very limited [3]. Thus, this Master's thesis aims to build an experimental set up in order to study dust dispersion and dust deposition behind an object in wind tunnel. This experimental set up is going to be the first step of further research in the same facility; that can be modified in the future according to necessities.

1.2 Key Terms; Wake, Dust Trail and Deposition

This study will be investigating dust trail and dust deposition characteristics by using optical methods. It is well known that when a fluid passes over an object, the flow becomes disturbed downstream of the object, and this region is called as the *wake*. Wake region can be divided into two subareas as near wake and far wake. The area just behind the body where the flow is separated is near wake. In this region, it is very common to see recirculation and the formation of a pair of streamwise longitudinal trailing vortices [4,5]. Downstream of the near wake is the far wake region where the largest-scale structures size increase [6], and the velocity field steadily decays [7].

Dust trail is the dust cloud which can be seen in near and far wake region of a moving vehicle. Dust is lifted from the road by mechanical mixing and buoyant eddies which occur due to passing vehicle [9]. Mechanical mixing and buoyant eddies can be fed by tailpipe, tires and body wake; these three elements are the energy sources for emission and dispersion. Figure 1 depicts these major energy transformation means and energy loses on a moving vehicle.

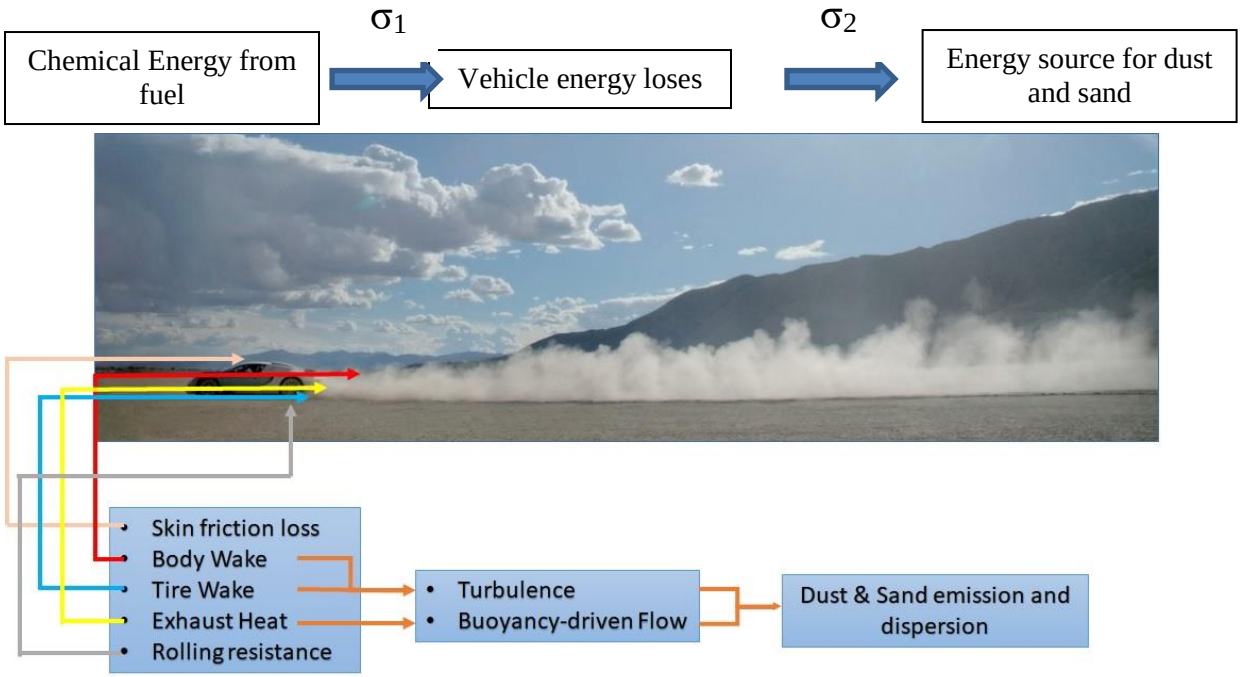

Figure 1: Schematic of energy transfer [8]

The dust cloud which constitutes dust trail is a mixture of pollutants as in the form of gaseous like exhaust gases and particulate matter, such as road dust and tire wear [7]. Furthermore, as in shown in figure 1, the dust trail takes its driving energy from a couple of different sources. However, time constraints limited the scope of this study. All of the

sources and pollutants are not included in this work. Therefore, this thesis only pays regard to body wake as dust trail energy source and road dust as a pollutant.

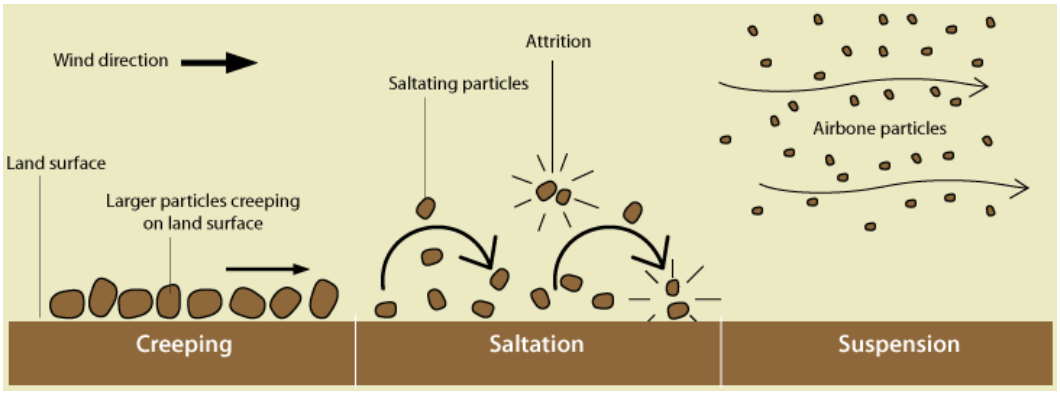

Figure 2: Deposition of dust particles [10]

Another key term is deposition of dust particles, which is portrayed in figure 2 [10]. Soil disturbed by a passing vehicle on an unpaved road is emitted as fugitive dust; the dust cloud is lifted and starts to travel downstream. First, this multiphase solid-air mixture is very dense, but after traveling downstream solid particles begin to lose their energy, and with the help of gravitational forces, they settle down to the ground again [9]. On the other hand, while dust particles are transported by vehicle wake, they can impact each other and be disintegrated to finer particles. Larger particles are impacted greater by gravitation. By contrast, finer particles are less affected by gravity, so they can suspend in the air longer and travel farther distances. This transportation process is known as *deposition*.

Chapter 2

Literature Review

2.1 Literature Review

It is significant to have a detailed literature review to comprehend dust emission and dispersion that stem from moving vehicle. At first glance, it readily seems that most researchers studying dust trail, dust emission, and dust dispersion due to a moving ground vehicle devote their effort to dust emission rates, utilizing active or passive sampling techniques, however, surprisingly dust clouds feature, and their dynamics grab little attention [11]. It is hard to find studies which specifically interested in dust cloud dynamics. Therefore, by splitting the dust trail problem into several building blocks, it might be easier to acquire meaningful fundamental knowledge from other more established issues. In this case, buildings blocks are fugitive dust emission, ground vehicle aerodynamics, heavy particle dispersion, and flow over cylinder which simplifies vehicle aerodynamics characteristics. The link connecting these building blocks is turbulent multiphase flow driven energy transfer.

Vehicle-generated fugitive dust emission is one of the main adverse effects on regional air quality [12,13,14]. Besides unpaved roads, mining areas, aggregate storage piles, agricultural tilling operations, and heavy construction operations are the other common sources for fugitive dust [13]. Although this wide range of source types grabs the

attention of researchers and institutions from various fields, the particle size-based classification of pollutants which is defined by the United States Environmental Protection Agency (EPA) under National Ambient Air Quality Standards is the most widespread. The Standards explain particle pollution, which is also called particulate matter or PM, as liquid droplets and microscopic particles that get into the air [15]. While PM_{10} refers to particles smaller than 10 micrometers in aerodynamic diameter, $PM_{2.5}$ defines particles smaller than 2.5 micrometers in aerodynamic diameter.

On the other hand, because PM was defined in 1987, earlier studies might refer to different particle size range definitions such as Total Suspended Particulate (TSP), Suspended Particulate (SP), Inhalable Particulate (IP) and Fine Particulate (FP) [13]. While TSP defines particles with a diameter between 30-100 micrometers, in successive order SP, IP and FP refer to particles with a diameter no greater than 30 micrometers, 15 micrometers and 2.5 micrometers [13].

Fugitive dust generation process can be summarized in two basic steps, first phenomena is pulverization of road material and production of wear particle by mechanical forces which come from vehicle tire, and the second step is entrainment of dust particles by turbulent vehicle wake [16]. When the road materials are squeezed between vehicle tires and earth ground, they tend to be pulverized into finer particles. This hypothesis has been investigated by Gillies et al. [17], and it showed that dust emission rates positively correlated weight of a car. However, their uncontrolled field environments and randomly-selected vehicles with no consistent aerodynamic shape leave a doubt on implication connecting weight and dust emission. Furthermore, Nicholson et al. [18] as in shown in figure 3, pictured that with the increasing particle size, particle resuspension percentage

are escalating. In this sense, it seems further studies are required to understand the relation between pulverization, particle size and dust emission.

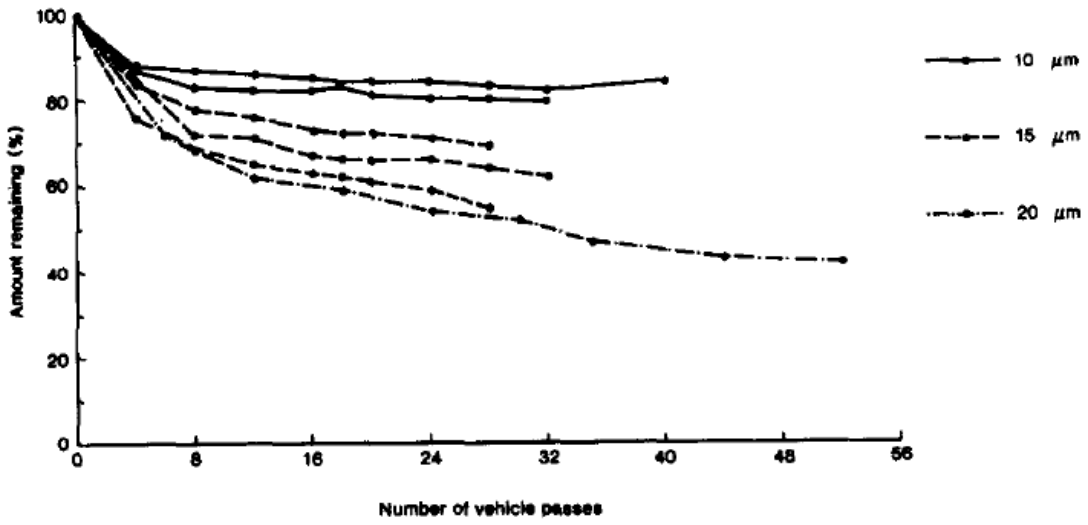

Figure 3: The resuspension of particles according to particle size [18]

Fugitive dust emission is also correlated with road conditions in many studies focusing on this area. Studies show that the amount of the suspendable material on the road, size ranges of particles, surface roughness, and moisture are the main attributes affecting dust emission rates [19,20,21,22,23]. Usually, soil surfaces are in the position of poor reservoirs for fugitive dust, and the suspendable material is diminished and does not last long. However, because of continuous disturbance by vehicular movement, strong winds or other human activities they may transform into very rich sources for fugitive dust [19].

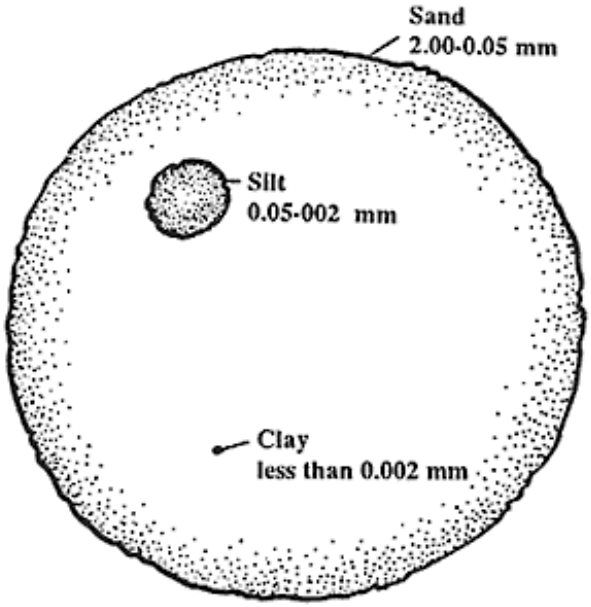

Figure 4: Relative size of sand, silt and clay [25]

Fugitive dust, which consists of soil can be in the various size of granular materials. Sand, silt, and clay indicate these size-based classifications in soil texture [24]. As in shown in figure 4 [25], while the sand particles are the coarsest ones, clay particles are the finest ones. Usually, larger and heavier particles have a smaller chance to mix in dust trail, instead of being lifted by the medium, more massive particles roll along the ground, which is described as surface creep [10]. On the other hand, tiny particles also cannot easily pull off from the surface by the wind [26], because of adhesive forces, cohesive forces and the gravitational forces [31]. Therefore, soil particles require a critical wind velocity, known as threshold velocity, to be initially disturbed [27]. As reported by Bagnold, below the threshold friction velocity no movement for soil particles is possible. In figure 5, Li et al. [28] depicted that dust particle size range which is more susceptible to dust emission due to lower threshold velocity utilizing Marticorena and Bergametti's [29] results.

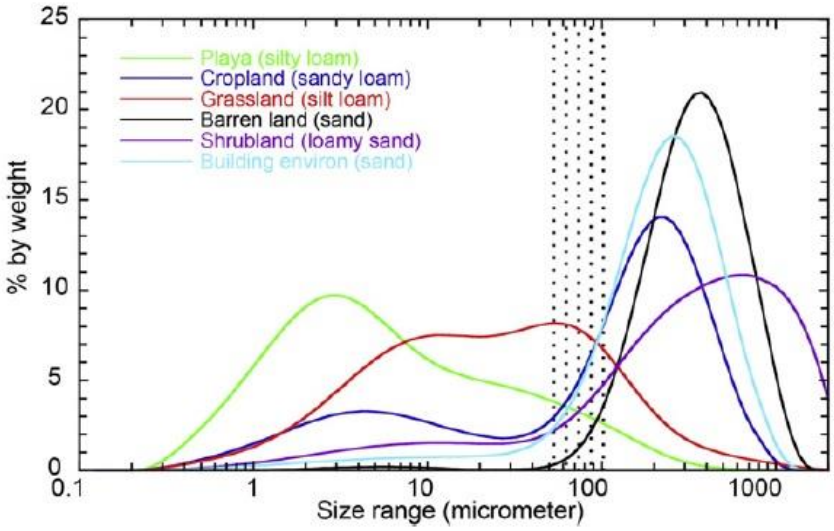

Figure 5:Particle size distribution of different lands. Dotted area represents lower threshold velocity [28].

Having lifted by the wind, particles settle down by gravitational forces, in this step particle size is important again. During the settling process, each particle reaches their terminal settling velocity with the help of the forces driven by wind and gravitation. Studies show that settling velocity increases with particle diameter or particle density [32,33]. As in shown in figure 6 [19,33], particles having smaller diameters tend to suspend in the air much longer.

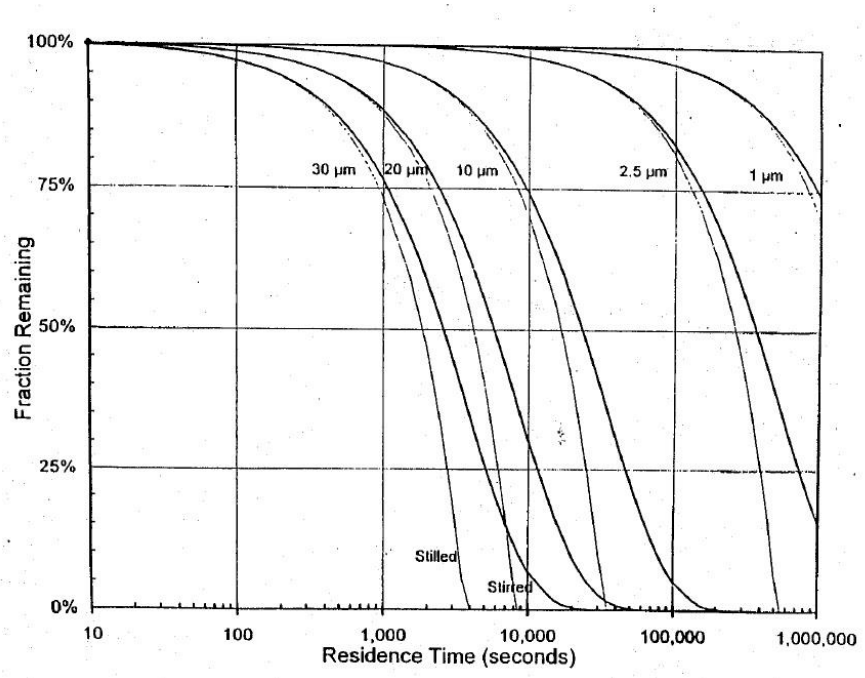

Figure 6: Settling time for different particle diameters [19,33]

Moisture level is another contributing factor in fugitive dust emission. The relation between erodibility and moisture of soil have grabbed attention for a long time [27]. Although in humid and sub-humid areas wind erosion takes place uncommonly, field studies show that arid and semi-arid regions are more frequently under the influence of wind erosion because of dry soil particles [34,35]. In moist soil, because of surface tension forces which stem from the water film distributed over soil mass, soil particles tend to stick to each other by these forces providing extra cohesion between them [36], instead of flying into the air. Thus, water or chemical dust palliatives, which absorb moisture from the atmosphere, are being used to reduce dust emission rates as the most common practice [37].

The second building block helping to understand dust trail problem is ground vehicle aerodynamic studies. Despite extensive studies on the aerodynamic characteristic

of ground vehicles which provide a deep understanding of the feature of wake-turbulence and flow structures behind a moving vehicle, there is a huge gap to connect those flow structure to dust emission and dispersion problem. According to the International Energy Agency [38], gas emissions with greenhouse effects will continue to go up parallel to rising fossil fuel usage, and emission rate will increase by about 57% between 2005 and 2030. Therefore, studies in this area mainly focus on drag reduction in order to decrease fuel consumption and increase efficiency [39,40]. On the other hand, the correlation between drag force, flow separation behind an object and turbulent wake is a well-known fact [41,42]. Boundary layer separation causes more drag force on the body, and flow separation also results in recirculation regions which are turbulent wakes, so researches try to decrease drag force by reducing flow separation and turbulent mixing wake [43,44,45].

Despite the lack of attention to the interaction between wakes and dispersion of pollutants [46], a unique study by Baker [7] that tries to connect flow and dispersion in ground vehicle wake covers the number of numerical, experimental and analytical results. In his work, Baker concluded that wake region could be separated into two subregions, namely near and far wake region. While the length of the near wake is up to 10 times a vehicle's height downstream of the vehicle trailing edge with usually consisting of recirculation region, large-scale flow structures and concentrations of longitudinal vorticity, the far wake; that shows steady downfall in wake velocities, is beyond near wake. Depending on the variety of frequencies, in the near wake region, various unsteady flow mechanisms can be seen such as instability associated with the separated shear layers, mechanism of wake pumping or large-scale instability of the complete wake structure. By contrast with this, in the far wake region, the majority of fluctuating energy is related to

overall instability of vehicle wake, instead of shear layer fluctuations. Furthermore, one of his most significant conclusions about the dispersion of pollutants within the near wake of vehicles is that the pollutant concentration field imitates the turbulence and velocity fields, and concentration variations can be seen that are aggreging with the fluctuations in the velocity field.

Although sand and dust are emitted into the air by rolling tires, they do not have a lot of chance to create a strong visible footprint without being dispersed into a large area by the turbulent wake. As it mentioned before, reducing turbulent mixing wake have been already aimed by researchers for a long time, so studies in this area help to reduce dust emission and dispersion in a limited way already. However, further considerations are still required for a deeper understanding of the connection between dust trail problem and aerodynamic features of moving vehicle.

Particle dispersion in turbulence subject is the third pillar of dust trail problem. Because of its importance in various natural phenomena and engineering applications, atmospheric [47] and turbulence science communities [48-50] have given noticeable attention to heavy particle dispersion in the past few decades [51]. Most works commonly divide dispersed two-phase flow, specifically particle-laden flow which is a solid-gas mixture, in three groups based on inter-particle collisions, to wit: collision-free flow (dilute flow), collision-dominated flow (medium concentration flow) and contact-dominated flow (dense flow) [52]. In the first type of flow, which is adequately dilute, fluid does not feel effect from the presence of particles, momentum exchange between particle and fluid can be considered in one-way, from fluid to particle, in this case, particles move in dynamic response to fluid motion [53], this is called one-way coupling. With increasing particle

volume fraction particle-fluid interactions alter dynamics of carrier phase, which is referred to as two-way coupling [54]. When the flow is dense enough four-way coupling, which includes particle-particle interactions as well, can be seen [55]. While one-way coupling requires less amount of computational time, the four-way coupling is challenging to model and solve in simulations [57]. When its particle concentration is considered, dust trail problem should involve four-way coupling. On that account, experimental studies are the good start point for dust trail problem.

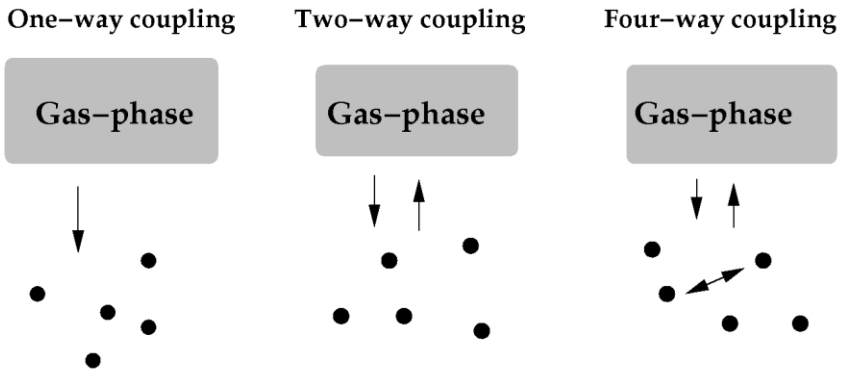

Figure 7:Schematic of different regimes [56]

When the time comes to the exercise to modeling two-phase flow which includes turbulent particle deposition, there are two possible approaches which are accepted generally. The Lagrangian approach is the first one, which is also known as the trajectory model, where the induvial particle's instantaneous moves are chased by calculating their equations of motions. The Eulerian approach is the other possible way to study particle deposition; this method is also known as the two-fluid model, where the particles are considered as a continuous phase. Particulate phase's motions are mathematically modeled by momentum, mass, and energy conversion, like a continuous phase fluid [58]. Our

experimental set allows us to track individual particles, so in this study Lagrangian approach will be adopted.

Most works in particle dispersion in turbulence adopted several assumptions for mathematical simplicity [59]. Reeks' assumption [60] where velocity field is Gaussian, homogenous, isotropic, stationary, and of zero mean is embraced in many studies [61-63]. While the velocity fluctuations are random but the average turbulence statistics are invariant in translation, the system is called homogeneous. The isotropic turbulence, which is first introduced by G.I. Taylor [64], means invariance under rotation of coordinate axes for turbulence statistics. In the theory, homogeneous and isotropic turbulence is idealized state of real turbulence [65], in other non-idealized turbulence, such as mixing layer [66] and channel flow [67] even the dispersion has been studied well, however, vehicle's wake is still relatively complicated comparing with these flows. In the turbulence of vehicle's wake, shear flow near the ground and bluff body wake in mid-air are expected as two different regimes. For such a complex flow, modeling is challenging for the dispersion statistics that is why an experimental study is needed for dust trail problem.

The last building block is "flow over a cylinder" which simplifies the vehicle's aerodynamic characteristics. Flow passing over a cylinder is one of the most studied cases, experimentally, computationally or analytically in the fluid community, as. Due to their basic and practical significance, a large number of researches have devoted their attention to the examination of steady cross-flows of general fluids over cylinders with circular, square and elliptical cross-sections [68]. Since the frontier work of von Karman, characteristic of different flows past a bluff body is well-known depends on Reynolds number [69], which is a dimensionless number as the ratio of inertia forces to viscous

forces. The fluid pressure increases from freestream value to stagnation point value, while the fluid comes to the front side of the cylinder. Because of the high pressure, fluid is forced to move along the cylinder surface, and boundary layers establish on both sides. However, viscous forces counteract on pressure force, and the fluid cannot follow the cylinder surface until the rear side of it and separates from both sides and form two shear layers. While the outermost part of the shear layer moves faster, on the contrary, innermost part of it moves slower, so the shear layers roll up. As a result, depending on the Reynolds number, different vortex street and wake patterns can be seen [70].

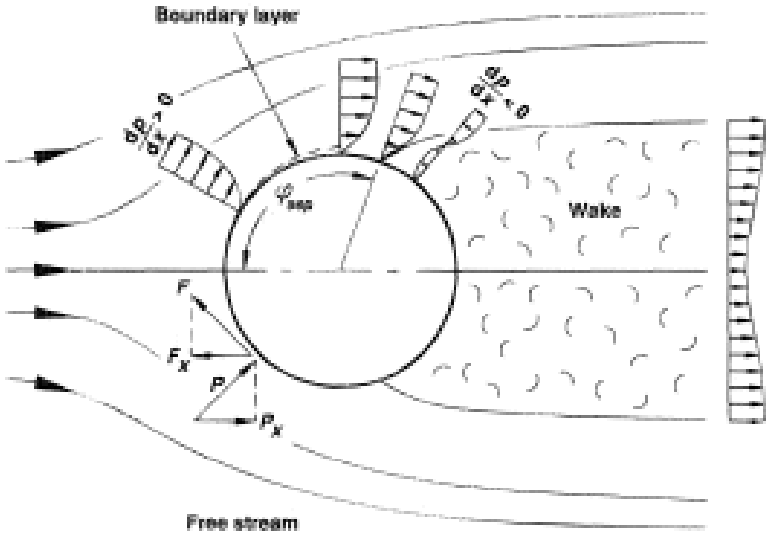

Figure 8: Flow separation [70]

On the other hand, the law of similarity which is developed by Reynolds suggests that if Reynolds number is close to each other for two cases with different flows around similarly shaped objects, flow pattern also should be close to each other [71]. Furthermore, the dimensional analysis method allows us to group variables into dimensionless parameters together which is used in fluid mechanics equations. Thus, a fundamental

relationship is developed between quantities with dimensionless groups and dimensions. After non-dimensionalizing governing equations, certain dimensionless groups appear such as Reynold number, Prandtl number, Weber number [72]. Similarities in these numbers for different cases also allow researchers to build a bridge between cases or simplify systems to less complex cases by modeling. In this thesis, vehicle bluff-body wake is simplified to cylinder wake utilizing the law of similarity method.

Chapter 3

Mathematical Background

The multiphase flow physics aspect of the dust trail problem remains largely unexplored, and the absence of major quantitative understanding makes it difficult to come up with reliable general method or model for dust emission and dust dispersion [82]. Thus, different empirical models, analytical approaches, and numerical methods exist in the literature. In this section, most cited ones will be introduced; in order to get a better understanding of the theoretical background and contributing factors to the dust trail problem.

3.1 Dust Emission Models

3.1.1 The EPA AP-42 Model

The U.S. Environmental Protection Agency emission model AP-42 was developed utilizing various linear regression analysis of emission factor test data versus parameters which change the intensity of particle emissions and still it is the most common predictor to estimate the emission of dust from unpaved roads. Although this empirical model for unpaved roads has been reorganized over the last three decades, every version of the equation shares significant common characteristics [83]. In here, the 1990 form of the AP-42 equation for unpaved roads can be seen:

$$e = 0.61\left(\frac{s}{12}\right)\left(\frac{S}{48}\right)\left(\frac{W}{2.7}\right)^{0.7}\left(\frac{w}{4}\right)^{0.5}\left(\frac{365-p}{365}\right) \qquad (3\text{-}1)$$

where e = PM_{10} emissions (kg/Vehicle Kilometer Traveled)

s = percent silt content of road bed

S= average vehicle speed (km/h)

W = average vehicle weight (kg)

w = number of tires (no dimension)

p = day number with ≥ 0.254 mm of precipitation.

Although, similar to reviewed and summarized papers in literature review section, this dispersion model takes into consideration vehicle speed, and weight, humidity, road material and tire number as the contributing factors for dust trail problem, vehicle aerodynamics is ignored.

3.1.2 The Gaussian Plume Equation

Another broadly used model is the Gaussian plume equation, which gives the concentration of a pollutant at (x, y, z) a time *t* from a point source:

$$C = \frac{Q}{2\mu u_h \sigma_y \sigma_z} . f . (g_1 + g_2 + g_3) \qquad (3\text{-}2)$$

where C (μg/m^3) is the pollutant's concentration at *x* m downwind from the road, *y* m distance from the crosswind source point, and z m height from the ground. Q (μg/s) is the source emission rate, u_h (m/s) is the horizontal wind velocity along plume centerline and σ_z and σ_y (m) are the vertical and horizontal standard deviations of the emission distribution, respectively. The crosswind and vertical dispersion parameters are f=exp(-$y^2/2\sigma_y^2$) and g=g_1+ g_2+ g_3, in order of;

$g_1 = exp\left(-\frac{(z-H)^2}{2\sigma_z^2}\right)$ is the vertical dispersion with no reflection,

$g_2 = exp\left(-\frac{(z+H)^2}{2\sigma_z^2}\right)$ is the vertical dispersion due to reflection from the ground and lastly,

$g_3 = \sum_{m=1}^{\infty}\left\{exp\left(-\frac{(z-H-2mL)^2}{2\sigma_z^2}\right) + exp\left(-\frac{(z+H+2mL)^2}{2\sigma_z^2}\right) + exp\left(-\frac{(z+H-2mL)^2}{2\sigma_z^2}\right) + exp\left(-\frac{(z-H+2mL)^2}{2\sigma_z^2}\right)\right\}$ is the vertical dispersion due to reflection from inversion lid aloft [84]. H (m) is the emission plume centerline height from ground and L (m) is the distance from the ground to the bottom of the inversion aloft. However, it should not be forgotten that this equation is for a single point source, while the road has a finite length as a line source. Thus, this equation must be integrated over the length of the road. On the other hand, this equation simplifies flow to highly idealized shape with homogenous and stationary turbulent. Furthermore, Gaussian plume equation considers natural atmospheric

turbulence more than vehicle's wake which is significantly important for dust trail. Therefore, this model is more accurate for farther away distances from the source.

3.1.3 Vertical Dust Concentration Models

Besides Gaussian distribution, there are other two types of equation exist for modeling the vertical change in dust concentration: a first-order exponential equation and a power law equation [12]. The first-order exponential decay model for dust concentration was described, that considering that the difference in eddy diffusivity with elevation is a power law function, by Goossens (1985) [73] as;

$$C(z) = exp(-Bz) \qquad (3\text{-}3)$$

The power law equation, which assumes a quasi-steady-state distribution of particles where the downward flow due to gravitational forces settling is balanced by the upward flow due to turbulent fluctuations, was derived by Goossens [73] again as;

$$C(z) = C_{ref}\left(\frac{z}{z_{ref}}\right)^{-Q} \qquad (3\text{-}4)$$

where Q is the fitting parameter and C_{ref} is the dust concentration measured at height z_{ref}. On the other hand, B is the empirical fitting constant which can be found in Goossens' work [73]. In Goossens' study, those fitting parameters include threshold velocity (m/s), deposition velocity (m/s), friction velocity (m/s), which is also called shear velocity, and k Von Karman's constant (k≈ 0.4).

To sum up, all different models considered various parameters which are described in the previous section; every model simplifies dust emission' physics ignoring different

effects. Briefly, humidity, vehicle speed, road material, sand and dust threshold velocities are considered as primary contributors.

3.2 Numerical Methods

Numerical simulation of turbulent particle-laden flow can be divided into three sub-categories; Direct Numerical Simulations (DNS), Large Eddy Simulations (LES) and closure models. In this study, these three methods will be briefly introduced, although extensive and more detailed review can be found in Mashayek & Pandya (2003) [74], Loth (2000) [75], Elghobashi (1994) [76].

3.2.1 Direct Numerical Solutions

Solving the governing equations without any models is called Direct Numerical Simulation. In DNS, all details of the flow and all scales are resolved and captured. However, these much details make DNS very expensive in terms of computational cost, and it becomes feasible only for simple geometries and low Reynolds number flows. Thus, this method is not practical for engineering applications, but it still comes in handy to get a physical understanding of particle-laden flows and can be helpful to the enhancement of closure models. Although, it is a common practice to treat flow as one-way coupled, in DNS studies, two-way coupling, which takes into account the feedback from the particles on the flow, can also be found in some studies [77-78]. In these works, to be able to

simulate solid particles by a Lagrangian approach, and to be capable of performing direct numerical simulations for gas phase, the following equations must be solved simultaneously, for gas phase;

$$\nabla . u = 0 \qquad (3\text{-}5)$$

$$\rho_g \left(\frac{\partial u}{\partial t} + u.\nabla u\right) = -\nabla p + \rho_g \upsilon \nabla^2 u + \rho_g g e_z + a_{ext} e_z + \frac{1}{(1-a_0)} f \qquad (3\text{-}6)$$

where u is the air velocity vector, p the periodic part of the pressure, e_z the downward pointing vertical unit vector, g is the gravity constant, a_{ext} (t) the external uniform streamwise pressure gradient component, and f the sum of the drag forces exerted by the particles per unit volume [78].

Furthermore, the motion of a single particle can be described in a Lagrangian way by;

$$\frac{dx_p}{dt} = v_p \qquad (3\text{-}7)$$

$$\rho_s V_p \frac{dv_p}{dt} = F_{d,p} + F_{c,p} + \rho_s V_p g \qquad (3\text{-}8)$$

where x_p and v_p are the location and velocity vectors of the particle center, respectively. In addition, V_p is the volume of the particle, while $F_{d,p}$ and $F_{c,p}$ represent the drag and collision forces on the particle respectively [78].

On the other hand, Vreman (2007) [77] and Li et al. (2001) [78] conclude the gas-phase turbulence is strongly suppressed by the particles and their particle-particle collisions. However, they do not have any information about how particle-particle collisions affect the settling time of particles.

3.2.2 Large Eddy Simulations

In LES, the large-scale eddies are explicitly calculated, and the small eddies are parameterized [79]. Removed small eddies can be modeled using a subgrid-scale (SGS) model. Thus, when it is compared to DNS, LES is less computationally expensive, therefore can be used for higher Reynolds numbers and more complex geometries. Similar to DNS studies, the dispersed phase of flow is computed using Lagrangian tracking in which particle motion is governed by the lift and drag force [80].

3.2.3 Closure Models

In closure models before solving the governing equations, they are averaged and modeled. This process makes closure model methods the least computationally expensive. Accordingly, this method becomes useful for engineering applications. However, averaging creates unclosed terms which are needed to be modeled. As mentioned before, two distinguished methods exist, the Eulerian-Eulerian way which considers the particle phase as a continuum similar to the continuous phase and Eulerian-Lagrangian approach that represent the particle phase as discrete particles. Although in the Eulerian-Lagrangian method, the number of particles is limited because tracking each particle is computationally more expensive compared to Eulerian-Eulerian approach, the Eulerian-Lagrangian method allows modeling more features of the particles such as wakes behinds particles, particle rotation and particle trajectory [56].

Both phases in the Eulerian-Eulerian approach are computed as a continuum phase which obeys conservation equations of momentum and mass. Conservation equations are averaged over control volume which is larger than an individual particle but smaller than a characteristic length scale of the fluid. These mass and momentum equations can be written as;

$$\frac{\partial}{\partial t}(\phi_k \rho_k) + \frac{\partial}{\partial x_j}(\phi_k \rho_k u_{kj}) = 0 \qquad (3\text{-}9)$$

$$\frac{\partial}{\partial t}(\phi_k \rho_k u_{ki}) + \frac{\partial}{\partial x_j}(\phi_k \rho_k u_{ki} u_{kj}) = \frac{\partial}{\partial x_j}(\phi_k \tau_{kij}) + \phi_k (-1)^k \frac{f_i}{\tau_p} + \phi_k \rho_k g_i \qquad (3\text{-}10)$$

where continuous phase and particle phase are represented by the index k=1 and k=2 respectively, ϕ is the volume fraction, ρ is the density, u is the instantaneous velocity, τ_{ij} is the stress tensor, g_i is the gravitational acceleration and f_i is the drag term.

Using Reynolds decomposition method, the variables can be decomposed to mean and fluctuation terms, for example, $u_i = U_i + u'_i$ where u_i is the instantaneous value, U_i is the mean value, and u'_i is the fluctuating part. However, this averaging leaves behind the Reynolds stress variable, like an unclosed term which can be closed by Boussinesq hypothesis. Although Boussinesq hypothesis creates the term eddy viscosity, it can be modeled through use of one-equation or more commonly by two-equation models with equations for both these quantities such as K−ω or K−ε models, where K is the turbulent kinetic energy, ω is the inverse time scale of the turbulence and ε is the energy dissipation rate.

3.3 Time-Averaged Mechanical Energy Equation for Turbulent Multiphase Flow

As mentioned previously, energy budget is vital to understand dust dispersion and emission, because some fraction of lost energy from the total energy is a source for dust emission and dispersion after a moving vehicle's wake. Thus, time-averaged mechanical energy equation for turbulent multiphase flow is required to be investigated.

Having been decoupled, the flow field can be written in mean and fluctuation features, as in mention above. Then, the Navier-Stokes equation takes the shape of the Reynolds- Averaged Navier-Stokes equation (RANS) for mean velocity and a separate momentum equation for fluctuation velocity. When both sides of RANS equation are multiplied by flow velocity, it is possible to extend those equations to describe the transport of mechanical energy. Chasing this idea, one can come up with the derivation of the time-averaged mechanical energy equation of multiphase flow whose derivation details can be found in the book of Thermo-Fluid Dynamics of Two-Phase Flow [81]. Although in the book, equations have been derived for two-phase heat transfer problems, e.g., condensation and boiling, dust trail problem is much simpler than these problems because of the neglectable amount of mass and heat transfer between the dust and gas phases. However, collisions between particles and pulverization are significant in denser flows. On the other hand, that phenomena is out of the scope of this experimental study, but it still has a potential future work.

The time-averaged mechanical energy equation for the k^{th}-phase in dust flow can be written as;

$$\frac{1}{2}\frac{D(\alpha_k\overline{\overline{\rho_k}}\hat{v}_k^2)}{Dt} = -\widehat{v_k}.\nabla(\alpha_k\overline{\overline{p_k}}) + \widehat{v_k}.\nabla.[\alpha_k(\overline{\overline{\tau_k}} + \tau_k^T)] + \alpha_k\overline{\overline{p_k}}g_k.\widehat{v_k} + M_k.\widehat{v_k} + \mathcal{L}_k \quad (3\text{-}11)$$

where the k=1 for dust phase and k=2 for gas phase, α_k is representing the time fraction of the kth-phase detected at a particular location, which is also related to its local volume fraction. Furthermore, while the double bar is representing the phase-averaged quantity, the hat is representing a weighted average.

Terms	**Physical meaning**
$\frac{1}{2}\frac{D(\alpha_k\overline{\overline{\rho_k}}\hat{v}_k^2)}{Dt}$	the material derivative of the mechanical energy of the kth phase
$-\widehat{v_k}.\nabla(\alpha_k\overline{\overline{p_k}})$	energy transport by pressure gradient
$\widehat{v_k}.\nabla.[\alpha_k\overline{\overline{\tau_k}}]$	energy sink to the viscous term
$\widehat{v_k}.\nabla.[\alpha_k\tau_k^T]$	energy exchange between mean and fluctuation components
$\alpha_k\overline{\overline{p_k}}g_k.\widehat{v_k}$	external force (gravity) induced energy conversion
$M_k.\widehat{v_k}$	energy source/sink term from force coupling between two phases; M_k represents the momentum source/sink.
$\mathcal{L}_k$	energy loss due to inelastic particle collisions

Table 1: Table of key terms in equation (3-11)

While the first six terms are experimentally accessible, $\mathcal{L}_k$ which quantifies the energy loss to heat that stems from inelastic particle collisions is not. Although, this term can be neglected in low concentration flows in which particle collisions events are rare, in denser flows it is a significant contributor to energy loss because of frequent dust-dust and sand-sand collisions.

Chapter 4

Experimental Setup

4.1 Overview of the Experimental Setup

In this work, deposition and dispersion experiments are performed in a wind tunnel which has a rectangular cross-section. The wind tunnel is a continuous indraft facility with a test section size of 47 x 31 x 305 cm. The tunnel provides a zero-pressure gradient flow for free-stream velocities from 0 to 27 m/s. This subsonic wind tunnel had been used to investigate boundary layer with low free stream turbulence, which has 0.3% free stream turbulence intensity, under normal conditions or it had been used for free stream turbulence studies with turbulence generator which can supply 60% turbulence intensity as high as and 10% as low as.

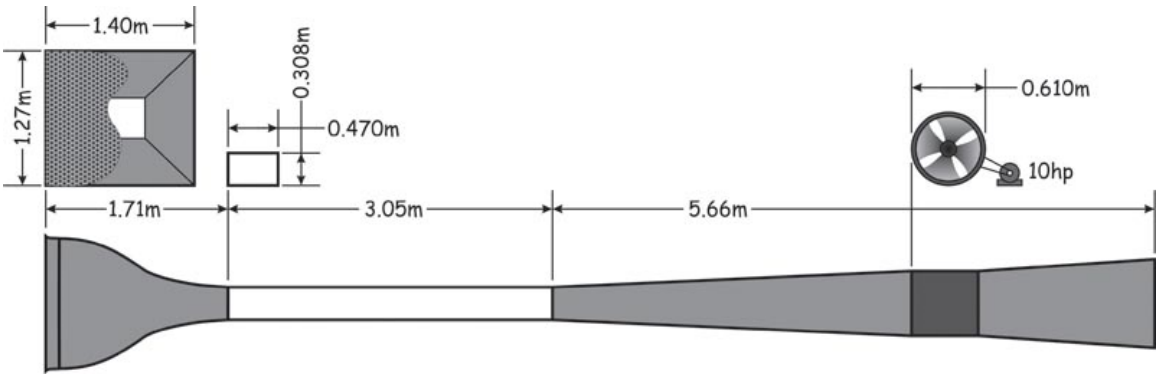

Figure 9: Schematic of Wind Tunnel

Since the tunnel was built with different purposes at first, some modifications are planned to make the wind tunnel more suitable to our case. When the tunnel was taken over, besides acrylic walls all around the test section, one side of the test section had been equipped with hot wires probe. Furthermore, the tunnel has an open-loop cycle. Although acrylic walls allow optical visualization of flows, hot wires probes were an obstacle to flow visualization. Thus, side walls modified firstly. On the other hand, the open-loop cycle is another issue, because the small dust particles can be hazardous for human health and they can damage the tunnel engine and fan blades. Therefore, to be able to collect to dust which is used in experiments, a filter housing system was designed. Additionally, connection parts that convert open-loop cycle to closed-loop cycle were modeled and built, in order to have more a developed and stable flow regime in the test section.

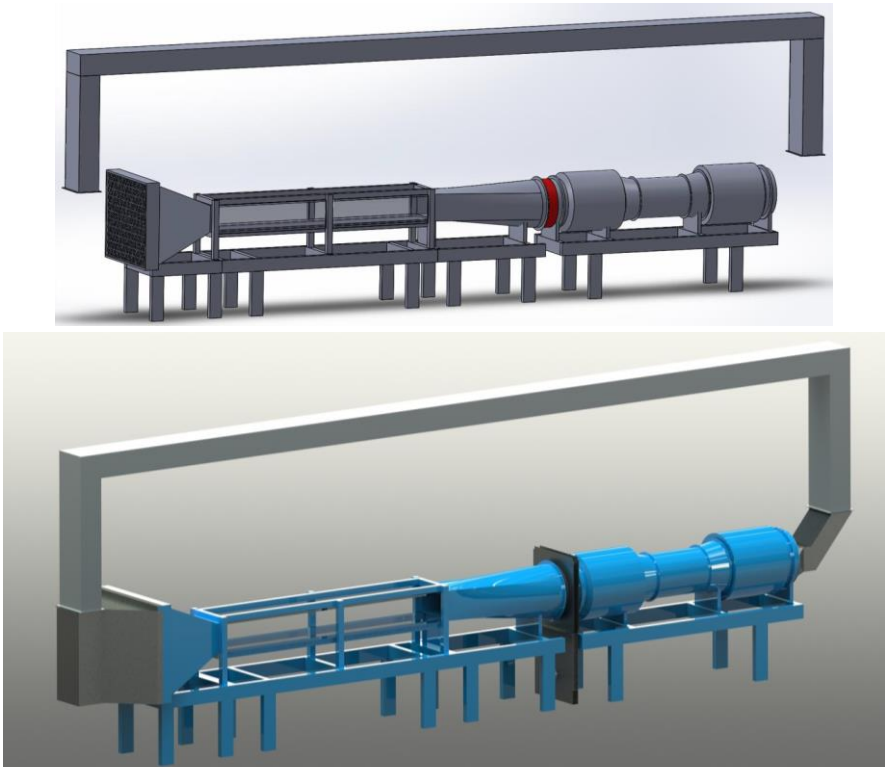

Figure 10: Top, CAD model of previous condition of wind tunnel, bottom after modifications

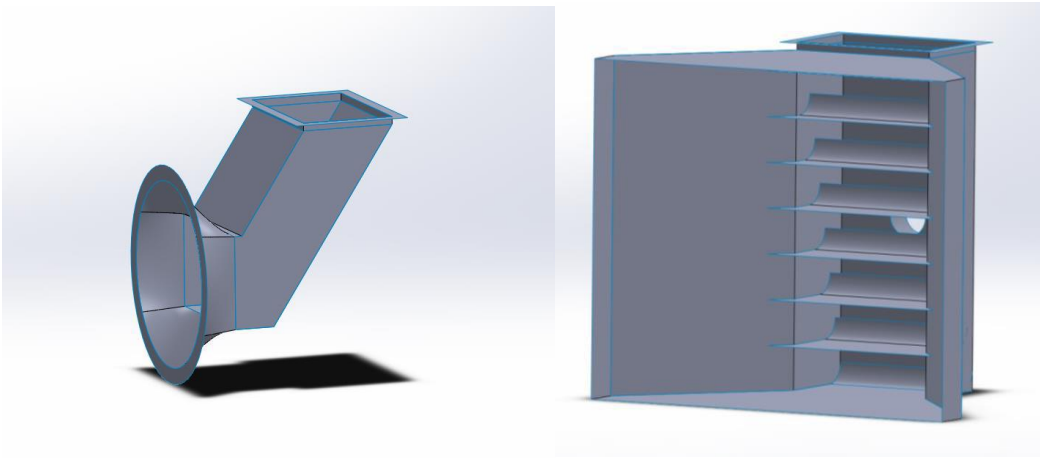

Figure 11: On the left, CAD model of rear connection part, on the right, CAD model of front connection part

Experimental studies require a lot of time to spend on design and manufacture of setups. Since our lab studies mostly experimentally, in order to gain some hands-on experience and improve to lab's group know-how knowledge in manufacturing processes for upcoming projects, first it was decided to build connection parts using university's facilities and by the participation of some members of the lab. In the manufacturing process, firstly, small structure elements were cut from main sheet metal plates. Secondly, they were bent, and shaped metal sheets were welded together. Despite, many hours of meticulous working, because of lack of experience in welding, connection parts could not be built in the desired level of quality, and in this time period couple months were lost. Thus, next, it was decided that work with outer supplier company.

Figure 12: Failed manufacture attempt and deformations due to thermal forces

In the next step, the frame, that holds visualization elements such cameras and light sources, was designed and built. 6 cameras and their light sources can be assembled on this cage, three cameras can be positioned from the side, and three others can look from the top. In the flow visualization studies, there are two different methods for lighting, one is backlighting, where light source and camera face each other so the shadow of particles can be seen, and the other is scattering lighting, where the particles scatter lights from light sources. For the velocity field experiments, high-speed cameras and light sources were mounted as the way which allows backlighting method. While the dust settling characteristics were studying, the DSLR camera and light source were mounted on the frame in the position that helps to utilize scattering lighting method.

One of main challenge in the flow visualization studies is the light source; it has to provide not only enough light to get images which are suitable for processing, but also homogenous light distribution over the field of view. Although laser light sources can correspond to these requirements, their exorbitant prices and extra safety measures, which are demanded to be able to use them, make them impractical for our case. Therefore, as an alternative option, LEDs are utilized as an illumination source. Various type of LEDs, including over-driven LEDs, were examined to find the most suitable one. While over-driven LEDs are supplying brightest light, they are not capable of providing uniform light density over the view area; the light is heavily denser in the center region. On the other hand, LED lamps, which were designed previously by one of our team member Jikang Shen, have the second brightest light and their rectangular shape that was cover an array of 4 x 7 LED bulbs are able to satisfy our expectation on homogeneity and power.

Polyamide particles, which are commonly used as a seeding material for PIV applications in liquids, were chosen as dust particles in order to eliminate uncertainties about dust cloud material as possible as because of their almost perfectly spherical particle shape and their standardized features. Polyamide particles, which have been used in experiments, have 60 μm mean diameter and their density is 1.2g/cm^3.

4.2 Experimental Procedure

The experiments, which were conducted in this study, can be divided into two sub-categories. First, in order to get velocity fields, high-speed cameras were used. Next, to be able to capture wider area and observe to dust settle down patterns, regular DSLR, Canon

EOS 650D, the camera was utilized. Even the cameras are different; the experimental procedure is the same.

In all cases, the wake was created by a cylinder which has 1.25 inches diameter. Furthermore, dust feeding occurred from a dust pile with a length and a width of 1.25 inches and with a height of 0.0625 inches, where it is located under the cylinder.

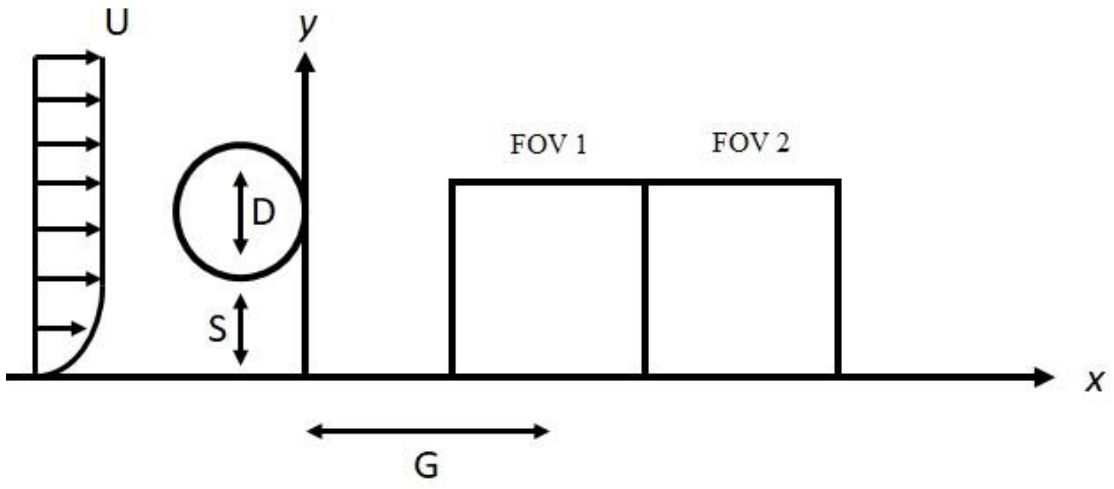

Figure 13: Schematic of experimental setup

In velocity fields experiments, two high-speed cameras were located adjacent to each other. In the schematic, FOV 1 stands for the field of view camera 1 and FOV 2 represents view area of camera 2, and they are 1.6 inches by 1.6 inches. For these cases, wind tunnel mean velocity, U, was set to 6m/s. In contrast, S, which represents height between the bottom of cylinder and wind tunnel bottom wall, and the distance between the center of view area and side of the cylinder, which was represented by G, are variables. By changing those values, it is possible not only to see how cylinder height affects the dispersion but also to observe different part of the wake.

On the other hand, DSLR camera, which looks from the top of the wind tunnel, allows to inspect wider area compared to high-speed cameras, and the individual particles

movement are not crucial for dust settle down patterns. Thus, we are not trying to capture dust particles movement step by step with Canon camera; this situation lets us increase free stream velocity, U. Furthermore, different cylinder positions on y-axis provide an environment to see how dust settle down patterns change depending on the height of the cylinder. Thus, the mean velocity of the wind tunnel and the height of the cylinder are two parameters which we looked for in the second step.

4.3 Limitations

As experienced previously on similar studies, optical access and light power are causing limitations in this study also. Especially for the high-speed cameras, light is a significant factor; higher frame rates are required to be able to capture individual particles movement. However, depends on higher frame rates, the camera is getting less light, this situation results as darker images, which are very hard to process. It is possible to reach 22500 frames per second with using our LEDs, but to attain higher frame rates more powerful LEDs or laser light sources are required.

On the other hand, increasing mean flow velocity only causes elongated particle images, because the same particle is captured by high-speed cameras in different places in the same frame. This also makes impossible for particles to be tracked. Thus, the free stream velocity and frame rate must be increased together, but as explained above, our limit in frame rate is 22500, so the maximum free stream velocity without seeing elongated particles is 6 m/s. Because of this reason, wind tunnel speed was set in high-speed camera observations.

Another significant limitation is the structure of the wind tunnel. Because of the support frame of tunnel walls, it was not possible to mount cameras in every position which was desired. Even in the best place of cameras, it can be seen that there is a darker area which stems from the support frame. This optical access issue was the one reason hinder us to study 3D.

Figure 14: Darker area in raw image

The second reason limited us to conduct experiments in 3D was the dust deposition itself. Dust particles which settle down aggregate on the bottom wall of the wind tunnel. Aggregated dust particles obstruct the view area from the top which is necessary to create 3D trajectories.

Chapter 5

Results

5.1 Experimental Conditions

In this study, dust deposition and dust settle down pattern tests have been performed in a wind tunnel facility to investigate effects of obstacle height and free stream velocity. In order to get data, the images were obtained by using two different kinds of cameras, high-speed camera and DSLR camera whose brand is Canon EOS 650D. The experiments were performed at room temperature. While the images were taken with high-speed cameras, free stream velocity was constant for all cases, in contrast, for dust settle down pattern tests were conducted in various free stream velocities which were between 6 m/s and 13.75 m/s. Table 2 shows Reynolds numbers for multiple cases, which were calculated based on the diameter of the cylinder, Reynolds number in the flow over cylinder is

$$Re = \frac{U.D}{\nu} \qquad (5\text{-}1)$$

where U is free stream velocity in (m/s), D is cylinder diameter in (m), and ν is the kinematic viscosity of the air (m^2/s), which is $1.516x10^{-5}$ in 20ºC room temperature. Besides Reynolds Number, table 2 summarizes Stoke numbers of dust particles, which is a significant indicator for dust particle movement. Stoke number is another dimensionless

number which is characterizing the behavior of particles suspended in a fluid flow, and it can be calculated using;

$$St = \frac{t_0 u_0}{l_0} \qquad (5\text{-}2)$$

where t_0 is relaxation time, u_0 is flow velocity, and l_0 is the characteristic dimension of the obstacle, in our cases, it is cylinder diameter. The particle relaxation time [85], t_0 is

$$t_0 = \frac{d_p^2 \rho_p}{18 \rho_g \nu_g} \qquad (5\text{-}3)$$

where d_p is particle diameter (m), ρ_p and ρ_g are the density of particle and environment fluid (kg/m^3), and ν_g is the kinematic viscosity of the gas (m^2/s). On the other hand, the boundary layer thickness is another critical parameter. However, direct measurement of boundary layer thickness was not possible on the experimental facility, so it was analytically calculated using 1/5 power law,

$$\delta = 0.373 * x * \left(\frac{U*x}{\nu}\right)^{-\frac{1}{5}} \qquad (5\text{-}4)$$

where δ is boundary layer thickness (m), and x is the location (m). Boundary layer thickness is one of the uncertainties about experimental conditions.

Cylinder Height (m)	Height/Diameter	Reynold Nu.	Stoke Nu.	δ (m)
0.003175	0.1	12655	2.45	0.039
0.00635	0.2	12655	2.45	0.039
0.009525	0.3	12655	2.45	0.039
0.0127	0.4	12655	2.45	0.039
0.015875	0.5	12655	2.45	0.039

Table 2: Parameters for velocity field experiments

Cylinder Height (m)	Height/Diameter	Reynold Nu.	Stoke Nu.	δ (m)
0.003175	0.1	12655	2.45	0.039
0.00635	0.2	12655	2.45	0.039
0.009525	0.3	12655	2.45	0.039
0.0127	0.4	12655	2.45	0.039
0.015875	0.5	12655	2.45	0.039
0.003175	0.1	16873	3.26	0.037
0.00635	0.2	16873	3.26	0.037
0.009525	0.3	16873	3.26	0.037
0.0127	0.4	16873	3.26	0.037
0.015875	0.5	16873	3.26	0.037
0.003175	0.1	20037	3.88	0.035
0.00635	0.2	20037	3.88	0.035
0.009525	0.3	20037	3.88	0.035
0.0127	0.4	20037	3.88	0.035
0.015875	0.5	20037	3.88	0.035
0.003175	0.1	24256	4.69	0.034
0.00635	0.2	24256	4.69	0.034
0.009525	0.3	24256	4.69	0.034
0.0127	0.4	24256	4.69	0.034
0.015875	0.5	24256	4.69	0.034
0.003175	0.1	29000	5.61	0.033
0.00635	0.2	29000	5.61	0.033
0.009525	0.3	29000	5.61	0.033
0.0127	0.4	29000	5.61	0.033
0.015875	0.1	29000	5.61	0.033

Table 3: Parameters for dust settle down experiments

5.2 Pre-processing

All images, which were taken during experiments, require a pre-processing step in order to get ready for data analysis. The first step in pre-processing is determining which pixel represents which location, to be able to do that a calibration target with many dots was used. Center position of dots is known, it is possible to determine positions utilizing this knowledge. In figure 15, the calibration target can be seen.

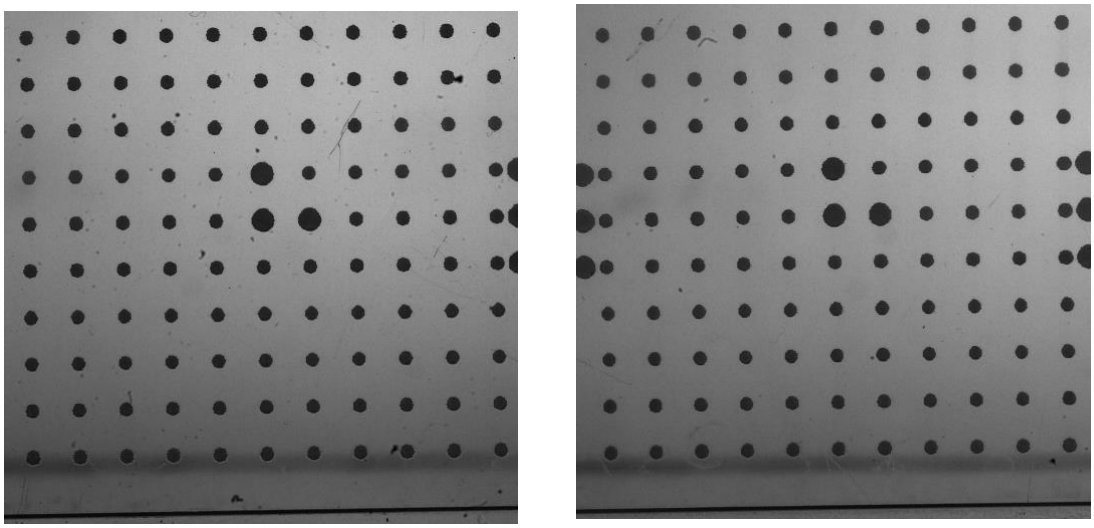

Figure 15: Calibration target image in view area 1 and 2

Raw images are not suitable to processed directly since background light, and background view are an obstacle to particle tracking code. Thus, removing background is necessary, so images, which come from high-speed cameras, were averaged by adding them together and they were divided to the number of images in order to get the background image. Having been calculated, the background image was subtracted from the raw image. In this way, pre-processed images, which are ready for data analysis, were obtained.

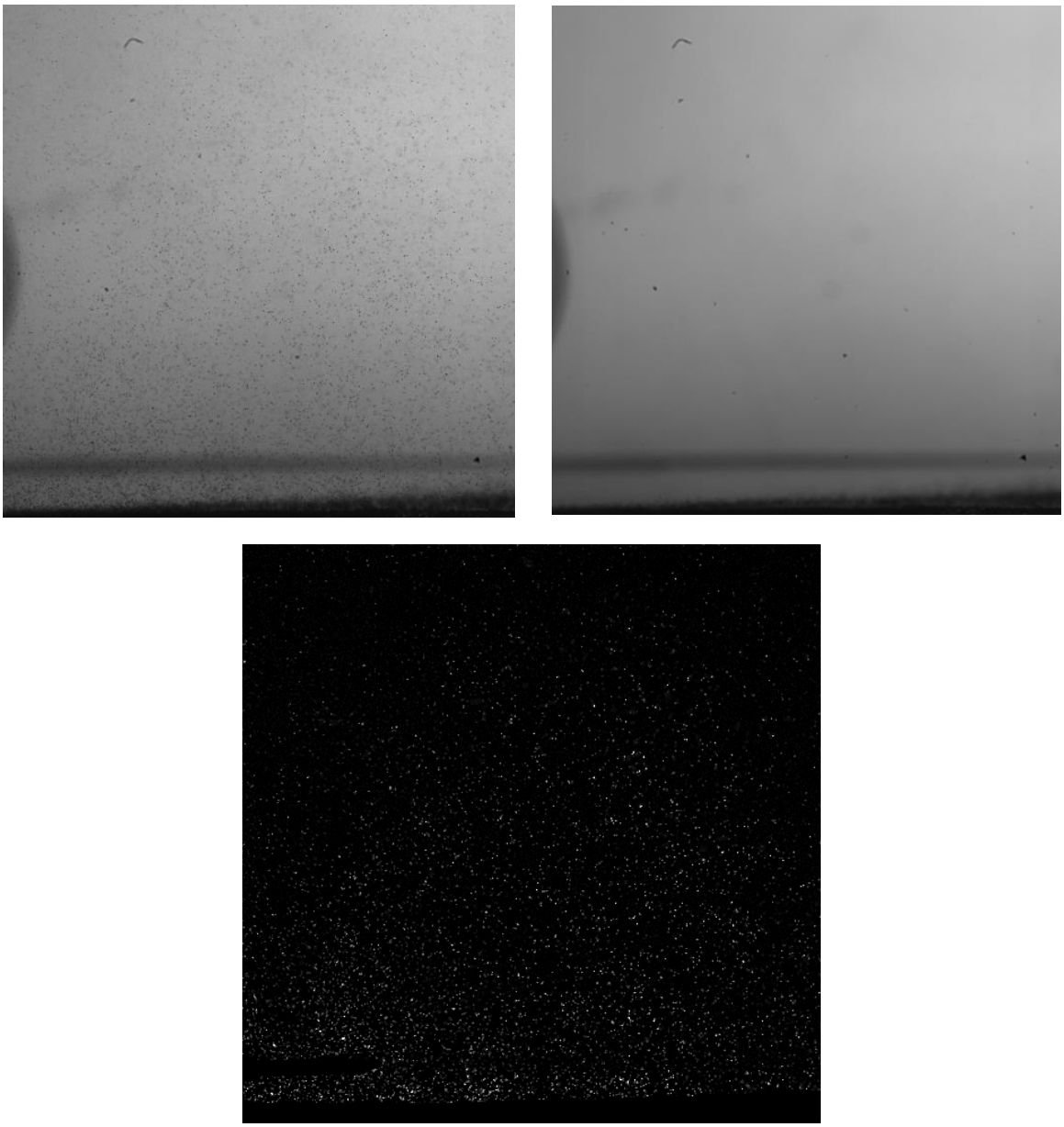

Figure 16: Top left, raw image, top right, background image, bottom pre-processed image

In figure 16, sample raw image, the background image which is average of 500 images and the result after subtraction of background from the raw image can be seen.

5.3 Velocity Fields

To get velocity fields of particles, in which wake behind the cylinder, 2D Matlab particle tracking code was heavily utilized. The code was written by Nicholas T. Ouellette in 2010, and it was updated by Douglas H. Kelley in 2011. 2D Matlab particle tracking code produces Lagrangian particle tracks using a predictive three-frame best-estimate algorithm. In the code, any pixel, which is going to be identified as a particle, must have a brightness that at least "threshold," the threshold value is important to distinguish to particle from noise. Having identified once, each particle is tracked using a kinematic prediction, and a track is broken when no particle lies within maximum displacement value which usually no longer than twice of mean diameter particles.

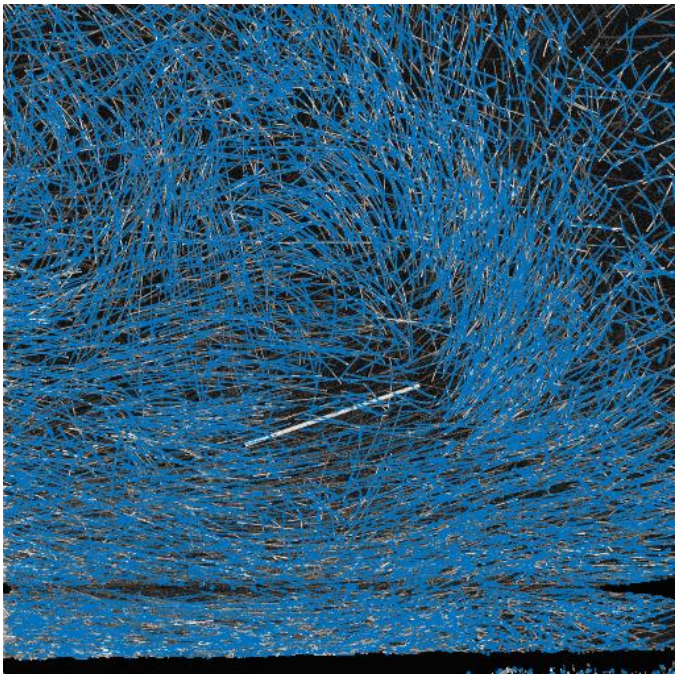

Figure 17: Unit velocity vector of particles

In the particle tracking code, the results are returned in horizontal coordinates, vertical coordinates, horizontal velocities, and vertical velocities of each particle. Thus, usually the number of particles are too much to see a meaningful result, this situation can be seen in figure 17. Because of this reason, the field of view divided into 32 by 32 grid, and for every average grid velocity was calculated by using individual particles velocity which is inside of that grid location.

Figure 18: Sum of images

On the other hand, there is no additional measurement in the experiments to visualize areas which do not contain particle in those regions, so the one should be aware that velocity fields show particle velocities which dispersed, not to complete wake region. Because of this reason, in velocity field figures some areas seem to have no velocity. In figure 18, 2500 images were summed together to show an example. Dark areas have no particle for the entire time, because of lack of particle entrainment to that areas, it will seem that those regions have zero velocity.

In literature, it is possible to see some works that studying for the wake structure of the circular cylinder with varying the gap height. Particle velocity fields results will be compared the studies which are summarized in table 4, that is adapted Wang and Tan 2008 [86].

Literature	Measurement tech.	Re_D	δ/D	$(G/D)_{crit}$
Bearman and Zdravkovich [87]	Pressure, hot-wire	$2.5\text{-}4.5\times10^4$	0.8	0.3
Grass et al. [88]	Visualization, hot-film	1785,3570	0.28, 2.6, 6	0.3 for δ/D <2.5; 0.5 for δ/D >3.5
Taniguchi and Miyakoshi [89]	Load cell, pressure, hot-wire	9.4×10^4	0.34-1.05	0.3-0.9
Buresti and Lanciotti [90]	Load cell	$0.88\text{-}2.7\times10^5$	0.1-1.1	0.4
Lei et al. [94]	Pressure	$1.3\text{-}1.45\times10^4$	0.14-2.89	0.4-0.2
Choi and Lee [91]	Visualization, pressure, hot-wire	1.4×10^4	0.35	0.3
Price et al. [92]	Visualization, hot-film, PIV	1200-4690	0.36	0.5
Wang and Tan [86]	PIV	1.2×10^4	0.4	0.3

Table 4: Summary of previous experimental studies on a circular cylinder close to a wall

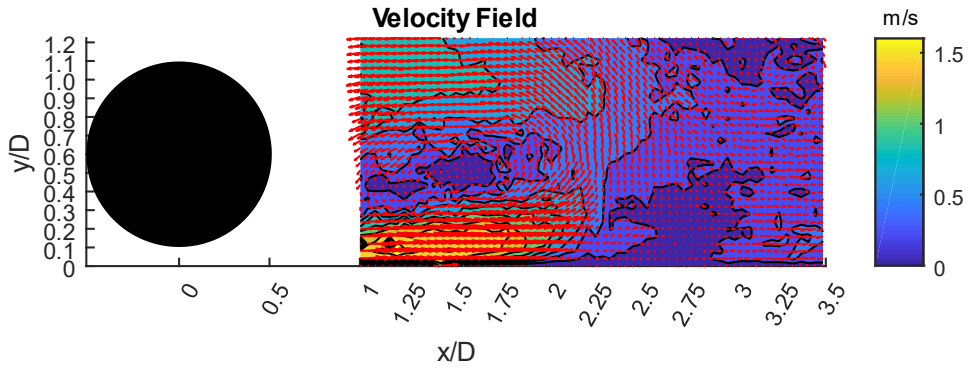

Figure 19: Dust particle velocity field G/D=0.1

In the figure, D represents the cylinder diameter and G depicts the gap between cylinder and wall. When the gap to diameter ratio is 0.1, a jet-like flow can be seen just below the cylinder; particles start to make a turn on counterclockwise direction by moving away from the cylinder. Previous studies show that it is possible to see a separation bubble after cylinder which has a length around 2-3 times of cylinder diameter in single phase flows, dust particles also show similar results, their recirculation region has a length around two times of cylinder diameter in the streamwise direction. On the top of the figure, backflow is seen, which is an indication of negative pressure, and it is in general agreement with Bearman and Zdravkovich's [87] measurements.

While the particles move along the streamwise direction, they start to lose their energy and especially particles which are close to wall seem suspended in a point, and after

that location, a backflow is seen. Furthermore, the backflow area and the region where particles recirculate look like emerging, and above that line, a chaotic distribution of velocity vectors is examined. Backflow region close to the wall is in agreement where the He *et al.* [93] shows the separation bubble on the wall. In contrast, to single-phase flow experiments, particles circulate in one direction in a separation bubble behind the cylinder.

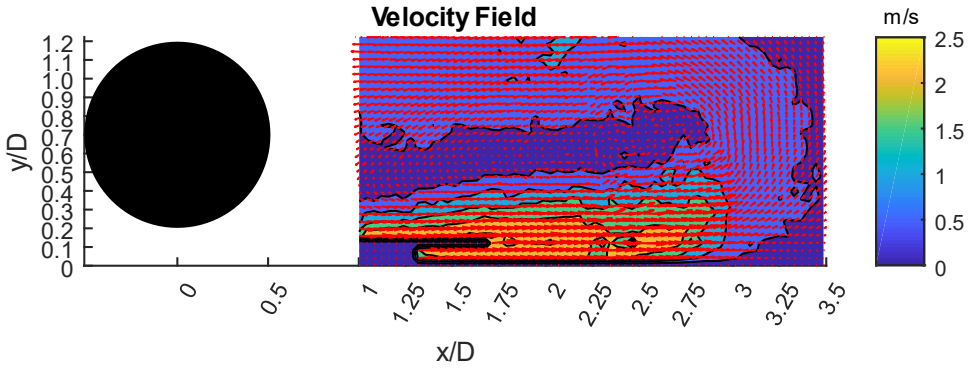

Figure 20:Dust particle velocity field G/D=0.2

When the gap to diameter ratio is increased to 0.2, gap flow rate is escalating. Particles seem to save their velocity in streamwise direction for longer distances. Furthermore, backflow region on top and gap flow region on the bottom come closer to each other, as expected separation bubble area was getting the higher point.

In figure 20, dust particles lose their energy and begin to make a circulation following counterclockwise direction; this turning radius center is further away from

cylinder than for the case at G/D=0.1. On the other hand, backflow is observed close to the wall region similar to the previous example. However, this time a chaotic region is not seen.

When, we continue to further away from the cylinder, in the area which is close to the wall, backflow is captured only. This backflow region is in agreement also where He *et al.* [93] calculates a separation bubble on the wall. Besides, the particles movement on the top part of the figure is similar to what they demonstrate.

In figure 21, close region to the cylinder is seen for the case gap to diameter ratio is 0.3. In this height of the cylinder, the jet shooting of particles is observed, the maximum value of velocity is higher than in previous cases. On the other hand, only a few particles entrain to higher altitudes; this shows vorticity is not dense enough to capture particles, in area close cylinder.

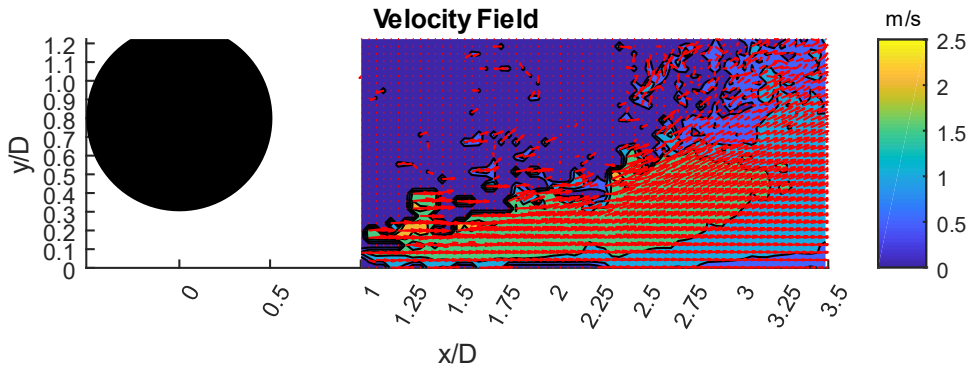

Figure 21: Dust particle velocity field G/D=0.3

Even for further distances in the streamwise direction, circulation area could not be captured. On the other, it seems particles continue to gain altitude by moving along the x-direction.

On the other hand, similar results were obtained for a higher value of gap to diameter ratio. As shown in previous studies, higher cylinder positions allow to more powerful gap flow. Separation bubble behind cylinder occurs higher elevations and the other separation bubble on the wall is diminishing, so we cannot capture backflow and circulation in our experiments above G/D=0.3.

At the case of the gap to diameter ratio is 0.4 and 0.5, stronger gap flow is seen. Thus, the dispersed particles start to climb in further distances from the cylinder. Also, due to the more powerful gap flow, particle velocities look higher. However, the amount of dust particle which is dispersed is getting lesser with increased cylinder height.

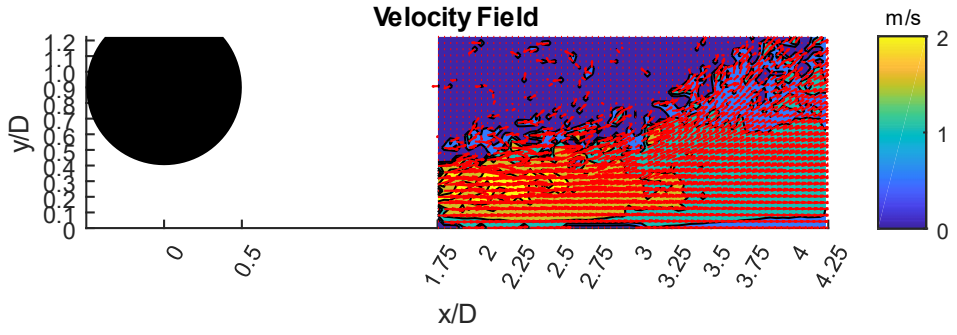

Figure 22: Dust particle velocity field G/D=0.4

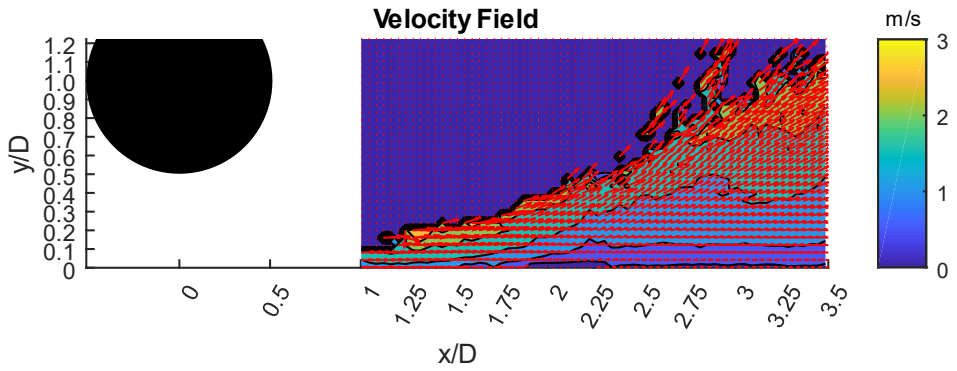

Figure 23:Dust particle velocity field G/D=0.5

5.4 Dust Deposition Patterns

Due to gravitational forces and pressure instabilities in turbulent wake region, lifted particles come down after a while by losing their energy. In this section, it was inspected how cylinder height and free stream velocity affect particle settling. First, the free stream velocity was kept constant, and the cylinder height was changed, to see the effect of obstacle height on particle settling. Next, while the object is in the same position, experiments were repeated in different free stream velocity, to see how dust settle down at different speeds.

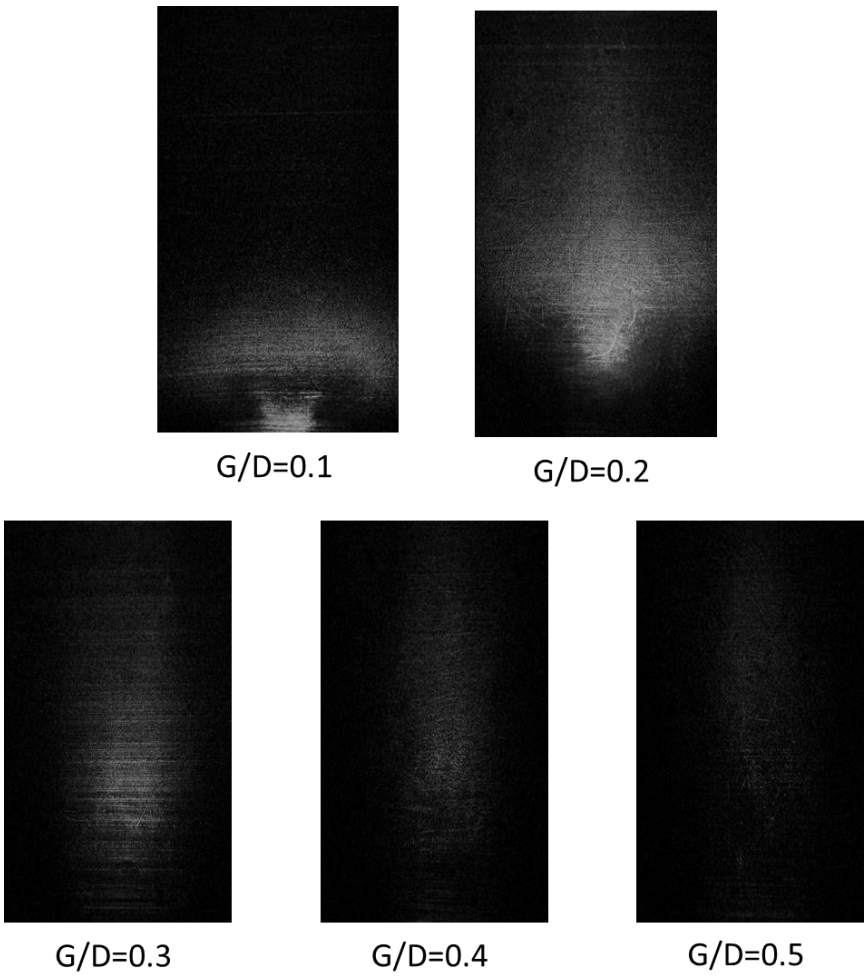

Figure 24: Dust deposition patterns for Re_D = 12655

In figure 25, dust deposition patterns can be seen for the different gap between cylinder and wall. Since, the images were taken from the top plane, in here dust particles which accumulated on the bottom are seen. The free stream air flows from the bottom part of the image to the top part, and the cylinder is attached to the bottom portion of images. Thus, down to up is x-direction which is streamwise and from center to left and right is z direction which is spanwise.

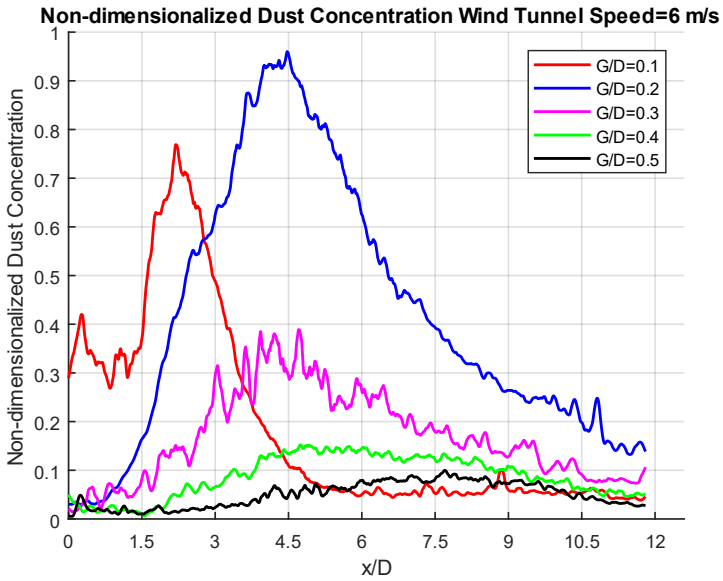

Figure 25: Dust concentration in streamwise direction for Re_D= 12655

Dust concentration in streamwise direction was calculated by using the brightness of each pixel in the image, firstly the image was considered as a matrix, and the pixel's brightness value adds up in the spanwise direction. Thus, a vector matrix was attained, whose every element represents a value for concentration in the streamwise direction. Finally, the brightest is accepted as maximum concentration, and darkest is considered as minimum concentration, by using these minimum and maximum values, nondimensionalization and signal smoothing were performed.

In very small gap ratios, G/D<0.125, particles are deposited much immediately behind the cylinder, this is indicating weakened gap flow which is also seen in Price et al. [92]. Both very small gap ratio and small gap ratio, 0.125<G/D<0.25, left behind a U-shaped deposition area first and then deposition region spreads in spanwise direction immediately for relatively small Reynolds number. This U-shaped region has leg length about to one and a half diameter of the cylinder, and its wideness is about the width of dust pile.

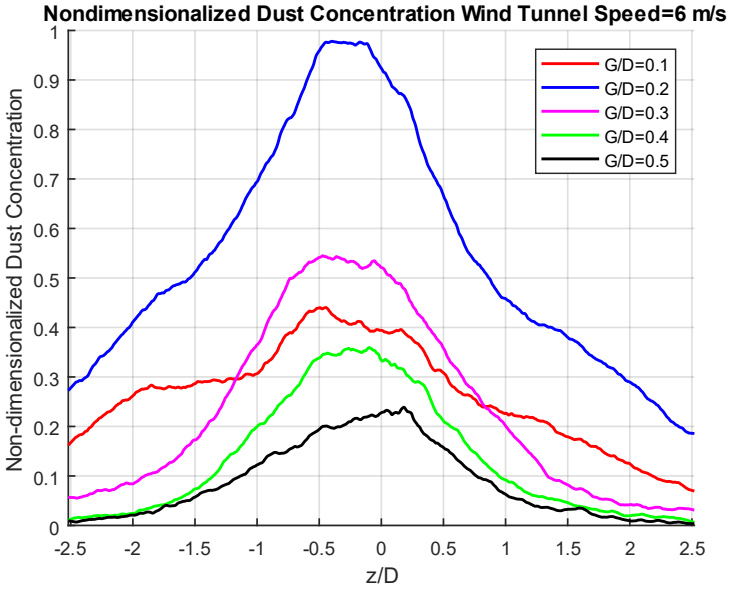

Figure 26: Dust concentration in spanwise direction for Re_D= 12655

Dust deposition concentrations were calculated by using the similar method that is utilized to calculate dust concentration in the streamwise direction. Along spanwise direction, it seems dust concentration mostly becomes dense around near to center region. Especially, for the gap-to-diameter ratio, G/D=0.3, and G/D=0.4, a Gaussian distribution can be seen along the z-direction. This shows that particles do not gain a much velocity to perpendicular to free stream flow, above a critical gap to diameter ratio.

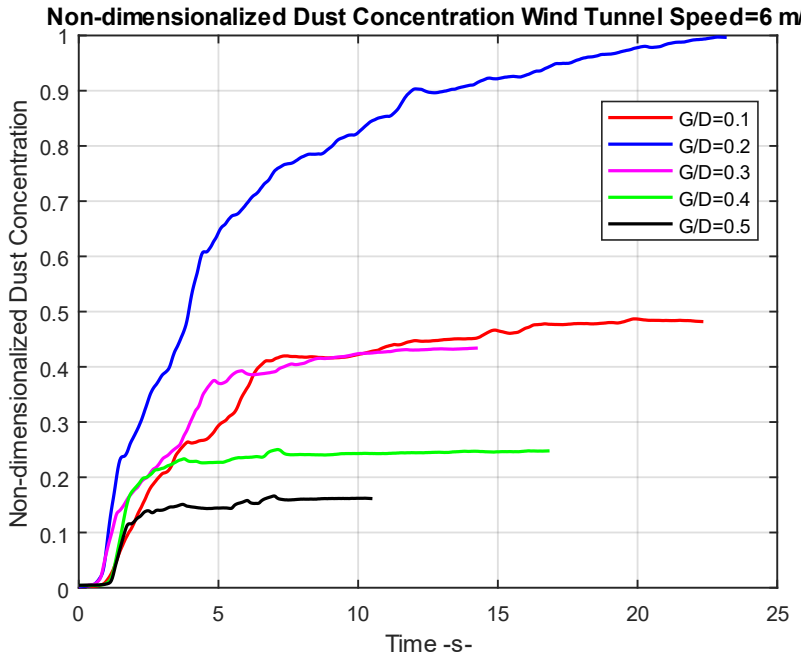

Figure 27: Time dependence of dust deposition for Re_D=12655

By adding each pixel value together in the field of view, dust concentration was calculated for each time step, and then nondimensionalization was performed. To reduce computation time, when the dust flow ends, data collection was stopped, so cases have different time in total. Starting from first seconds, dust concentration is increasing in all cases in this Reynolds number, this shows dust particles continue to collect on the bottom, and still, there are particles in dust pile, and it did not run out. Dust concentration amount is similar in G/D=0.1 and G/D=0.3, as mentioned, weakened gap flow obstructs air flow and dust dispersion in the very small gap to diameter ratio. On the other hand, higher cylinder position results in less vorticity in the region just beneath cylinder [93], because of this, dust amount, which can be lifted by air flow, decreases. This is supported by the results for G/D=0.4 and G/D=0.5, increasing in cylinder height turns as the reduction in dust dispersion.

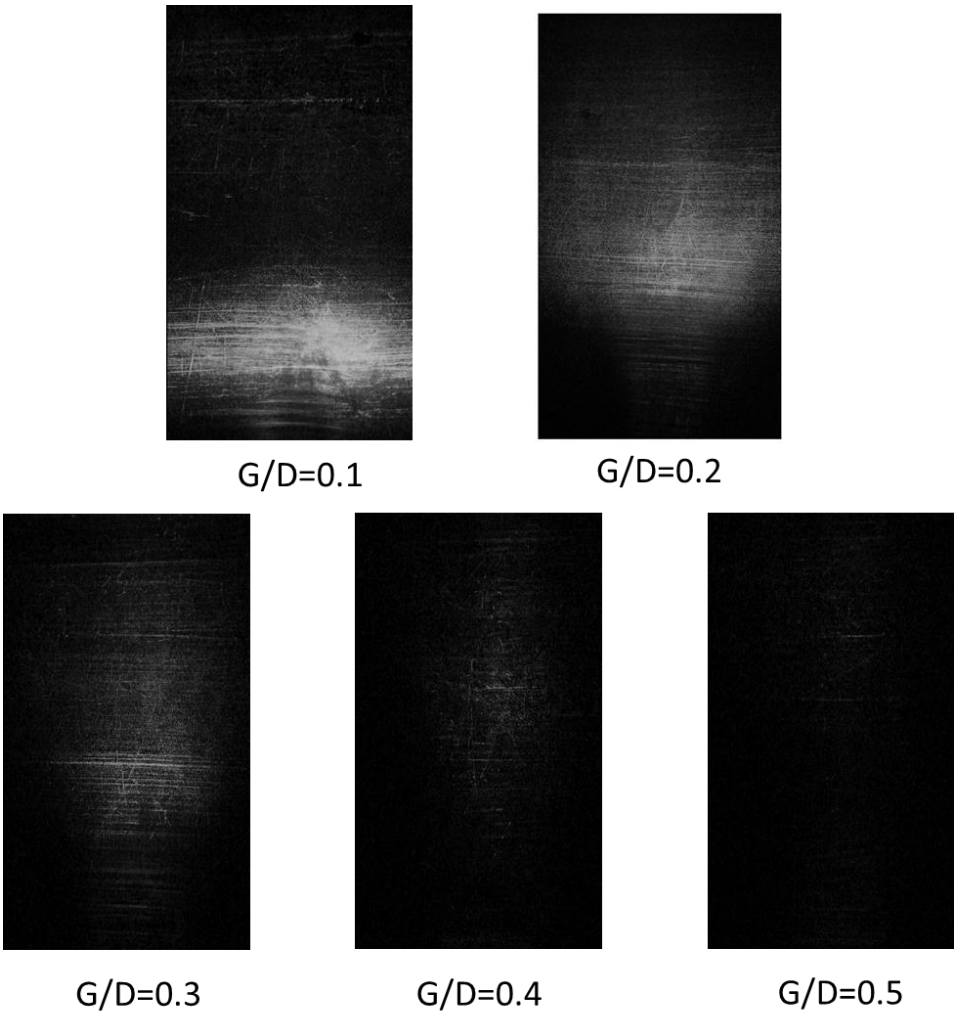

Figure 28: Dust deposition patterns for Re_D = 16873

When it is compared to previous cases, it is realized that the number of accumulated particles is increased. While the U-shaped deposition area is diminishing for G/D=0.1 case, it still can be slightly seen in G/D=0.2 case. However, this time the transition from the U-shaped area to the main deposition area is smoother.

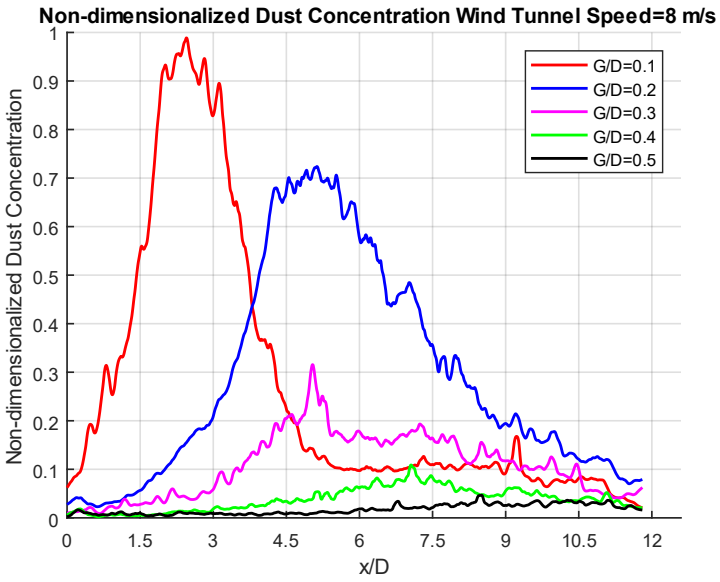

Figure 29: Dust concentration in streamwise direction for Re_D= 16873

Due to weakened gap flow and backflow, very small gap to diameter ratio case results in dust settling again right after cylinder. This shows a similar result to Bearman and Zdravkovich's study [87], where the negative pressure is more effective when the cylinder closes to the wall. Furthermore, increasing free stream air velocity lifting more particles.

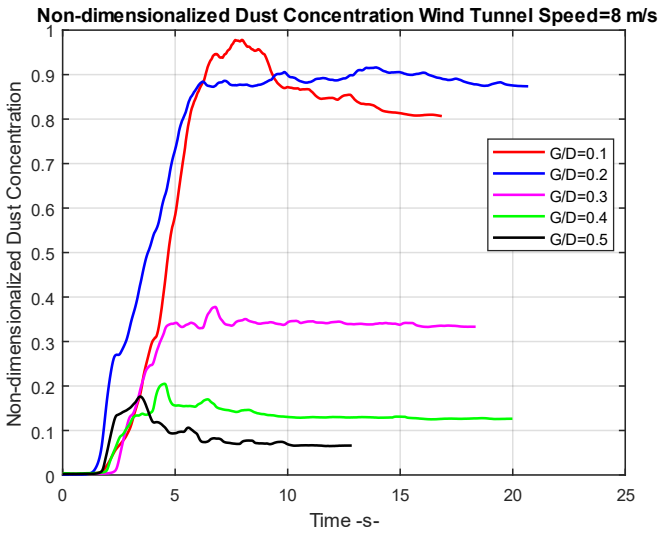

Figure 30: Time dependence of dust deposition for Re_D=16873

In time dependence graphics, a constant tail in horizontal direction shows that the dust lifting process ends. That happens because of two reasons, first, gap to diameter ratio is small enough, or air flow velocity is high enough to create negative pressure to lift all dust pile. Second, gap to diameter ratio is too much, or wind tunnel airspeed is too less to generate enough negative pressure and vorticity to lift dust particles sufficiently. These two situations can be distinguished by looking the highest points of lines, where the higher highest point is indicating run out of dust on the pile, lower highest point shows negative pressure is not enough to lift particles. Thus, it can be understood that when G/D=0.1 and G/D=0.2 dust pile completely was lifted, for higher values of G/D dust particles could not find enough power to disperse, and only lose particles on top of dust pile were lifted. On the other hand, G/D=0.1-line decreases after its highest point; this indicates that secondary lifting process from the main deposition area after particles settle down. This trend also can be seen for G/D=0.5. Furthermore, even both two highest value of G/D have similar peak points in dust concentration over time, G/D=0.5-line decreases more this indicates that stronger gap flow in the higher ratio of gap to diameter, that can also be seen in Wang and Tan [86] and He et al.[93], does not allow sediment particles to be deposited behind the circular cylinder. On the other hand, dust concentration is decaying sharply between G/D=0.2 and G/D=0.3, that reminds previous studies which found the critical number of the gap to diameter ratio as around 0.3.

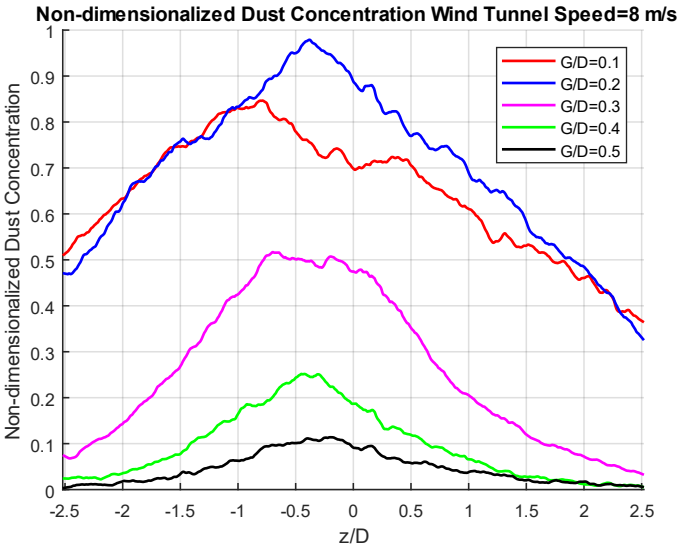

Figure 31: Dust concentration in spanwise direction for Re_D= 16873

Similar to the previous figure for dust concentration in the spanwise direction, G/D=0.3 and G/D=0.5 show the normal distribution in this one also. However, small gap to diameter ratios have higher values for dust concentration on ends; even for G/D=0.3, a slightly more spread distribution can be seen. Because of increasing Reynolds number, dust particles begin to gain more velocity in spanwise direction depends on turbulent interactions. Furthermore, this trend continues for higher Reynolds number.

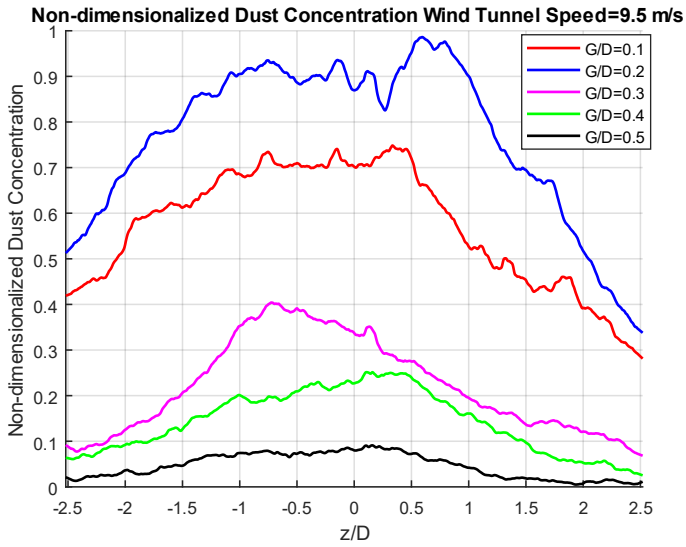

Figure 32: Dust concentration in spanwise direction for Re_D= 20037

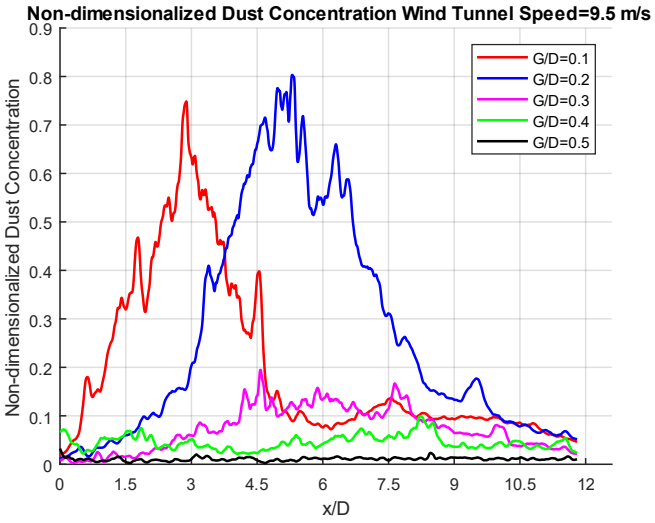

(a)

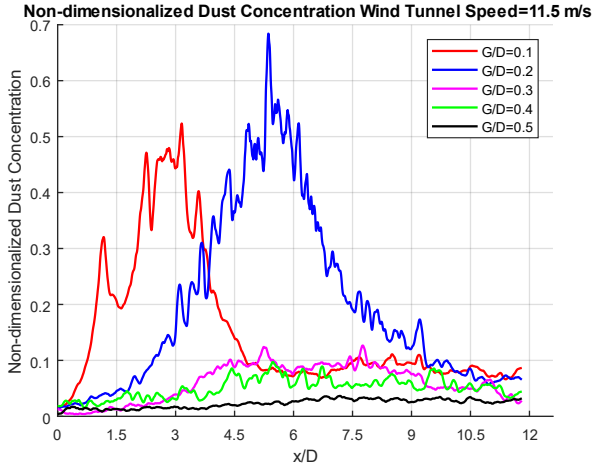

(b)

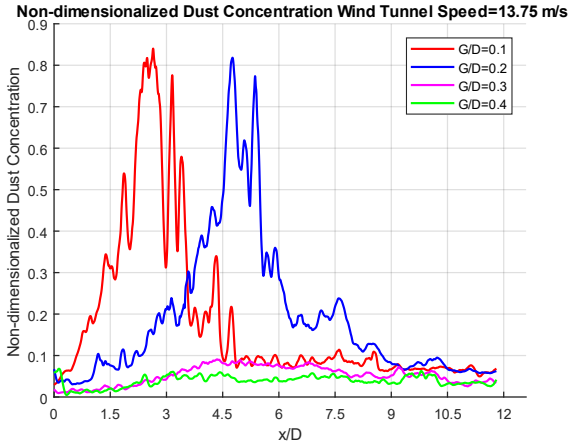

(c)

Figure 33: Dust concentration in streamwise direction for (a) Re_D= 20037, (b) Re_D=24256, (c) Re_D=29000

In figure 34, dust concentration in streamwise direction sharply decreases in G/D=0.3 position for all different Reynolds numbers so that it can imply to the critical number of the gap to height ratio is around 0.3, similar to previous studies.

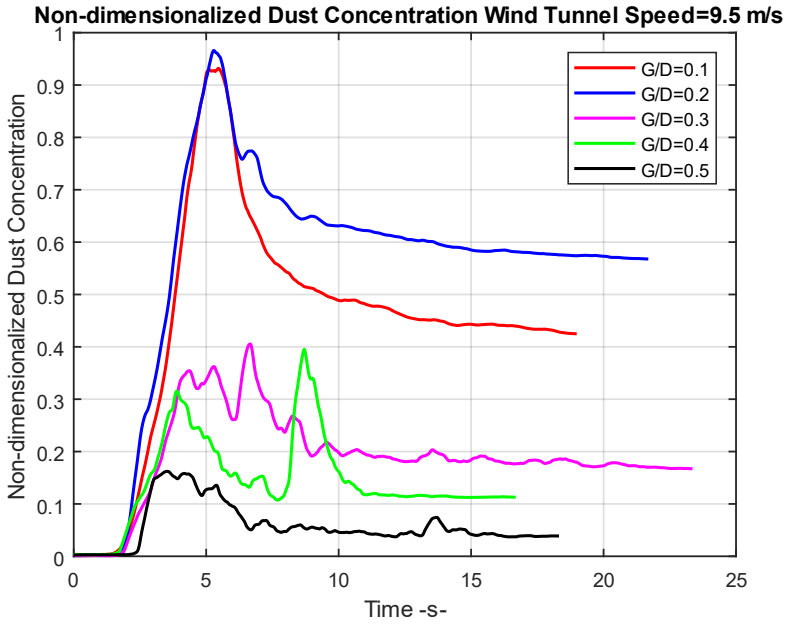

(a)

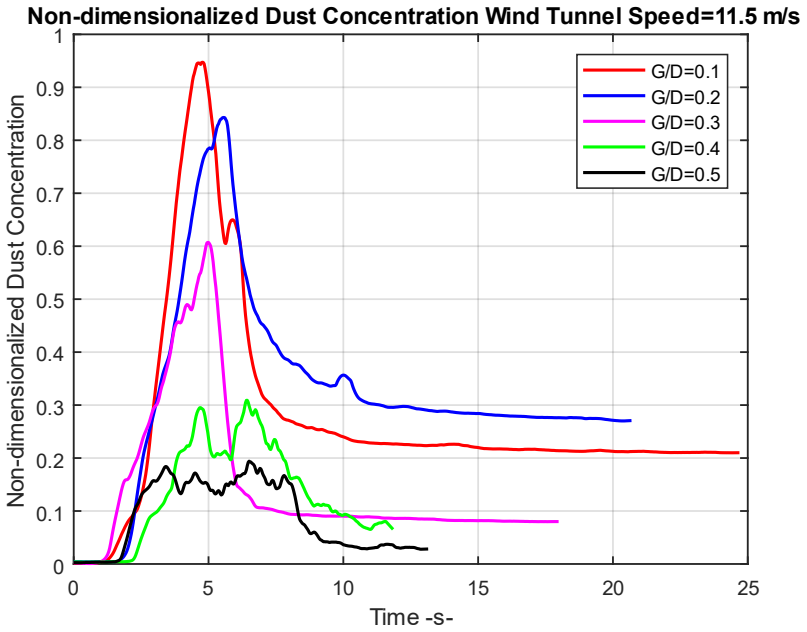

(b)

Figure 34:Time dependence of dust deposition for (a) Re_D= 20037, (b) Re_D=24256

On the other hand, when it is investigated, dust concentration depend on time looks like in figure 35. Decrease after a peak at G/D=0.1 and G/D=0.2 for both Reynolds numbers show dust particles in a pile completely were lifted, and more and continuing diminishing in dust concentration in G/D=0.1 imply secondary lifting from deposition area. This secondary lifting is expected more at smallest gap, because He et al.'s [93] velocity map shows while there is jet region for gap flow between half times to two times of cylinder diameter in downstream, in contrast, because of separation bubble on wall, the air velocity is too small for in the region two to six times of cylinder diameter in downstream, the location also the main deposition area for G/D=0.2. Another interesting result is to see two peaks when G/D=0.4, it implies there is a transition point for continuous dust lifting. However, that two peaks situation only appears for G/D=0.4 at the case of Re_D= 20037 and Re_D=24256 in our experiments. Thus, the transition point should be related to gap to diameter ratio and Reynolds number together.

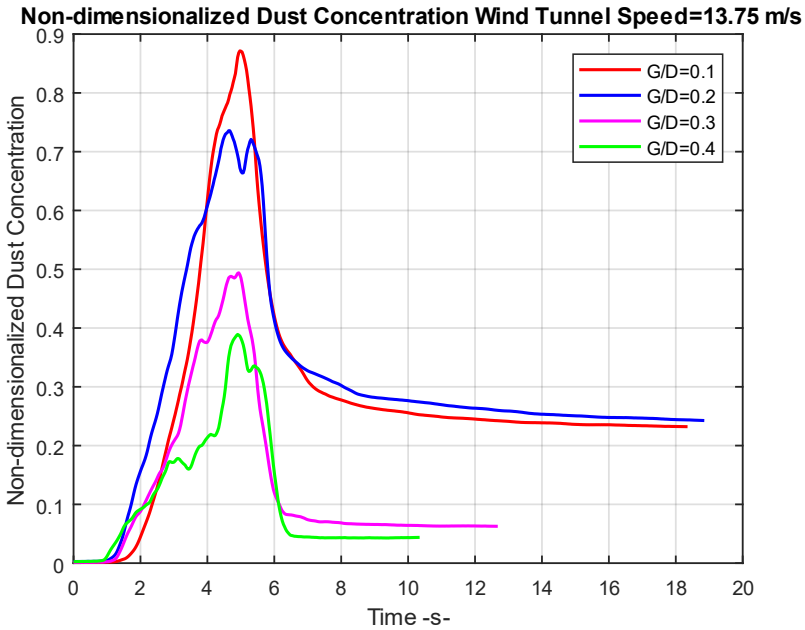

Figure 35: Time dependence of dust deposition for Re_D= 29000

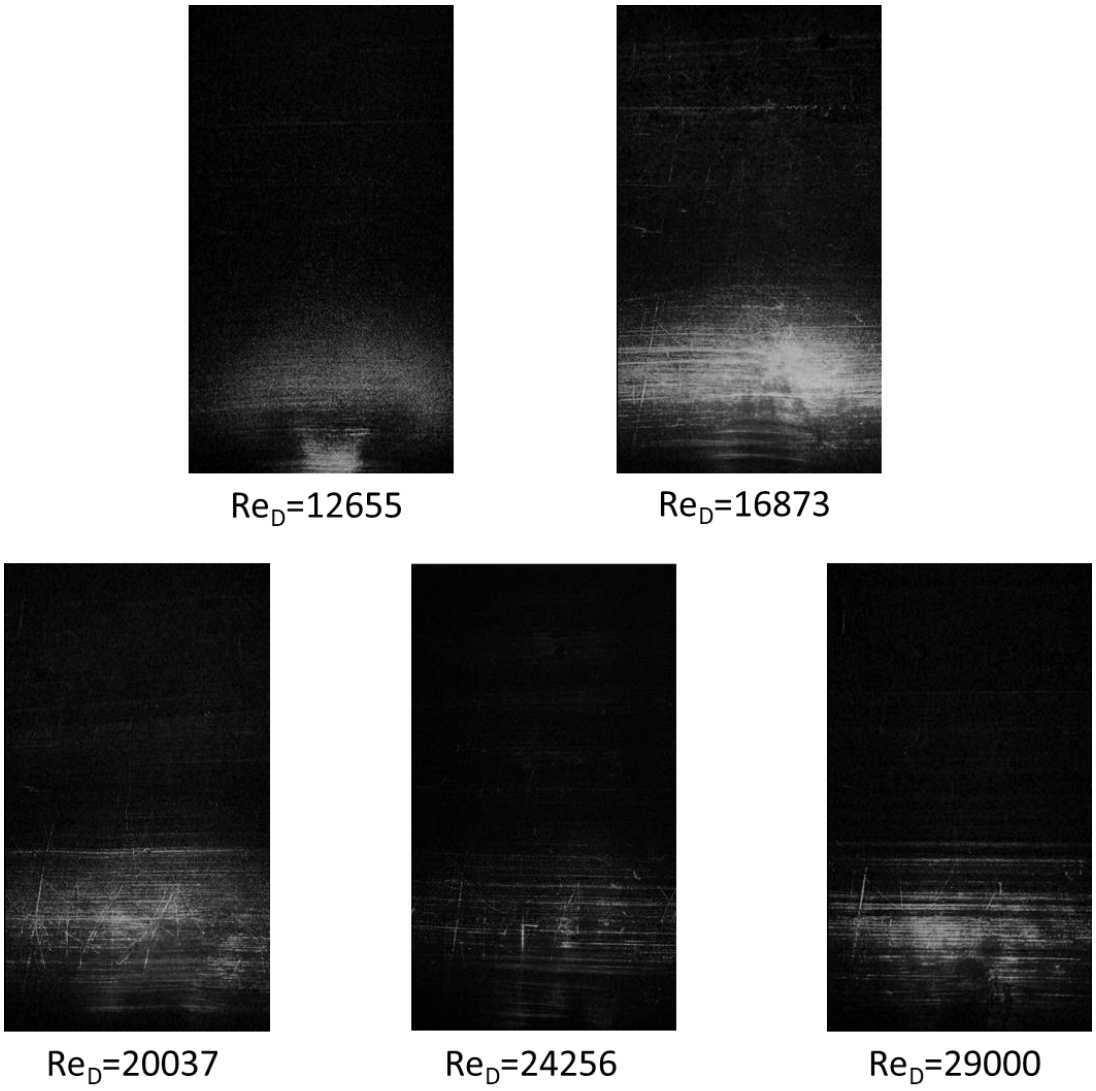

Figure 36: Dust deposition patterns for G/D=0.1

To be able to see how Reynolds number affects dust deposition patterns, in the next step, the results were compared by keeping the gap to diameter ratio same but changing wind tunnel airspeed, in other words, Reynolds number. At first glance, it is readily seen, at the case of G/D=0.1, main deposition area covers almost the same location in all different Reynolds numbers.

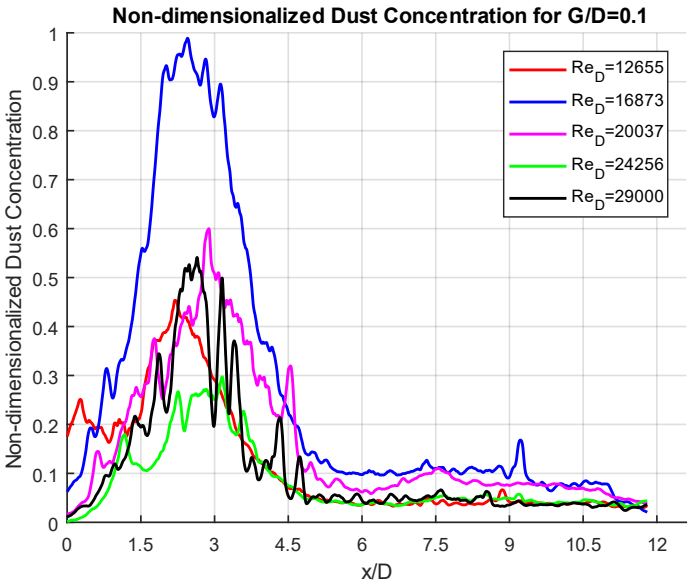

Figure 37: Dust concentration in streamwise direction for G/D=0.1

Figure 37 shows dust deposition area is located between half diameter of the cylinder and four and half times of cylinder diameter in downstream for all the cases at G/D=0.1. Maximum dust accumulation shows up when Reynolds number is around 17000. Most likely this is happening because the airspeed is high enough to lift all dust pile, but it is also low enough to let particles to settle down. This thought is supported by also figure 38.

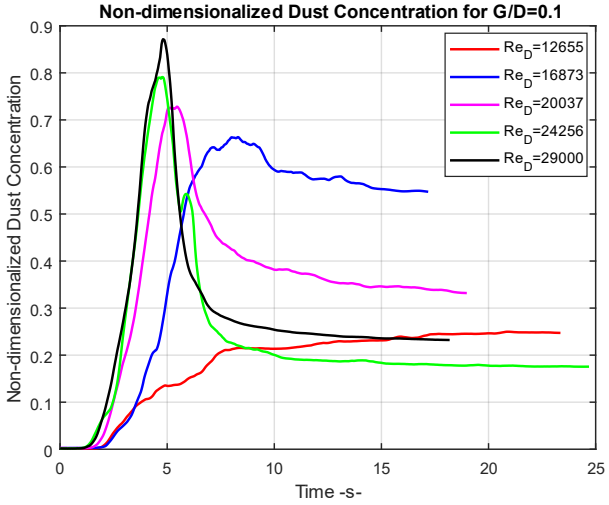

Figure 38: Time dependence of dust deposition for G/D=0.1

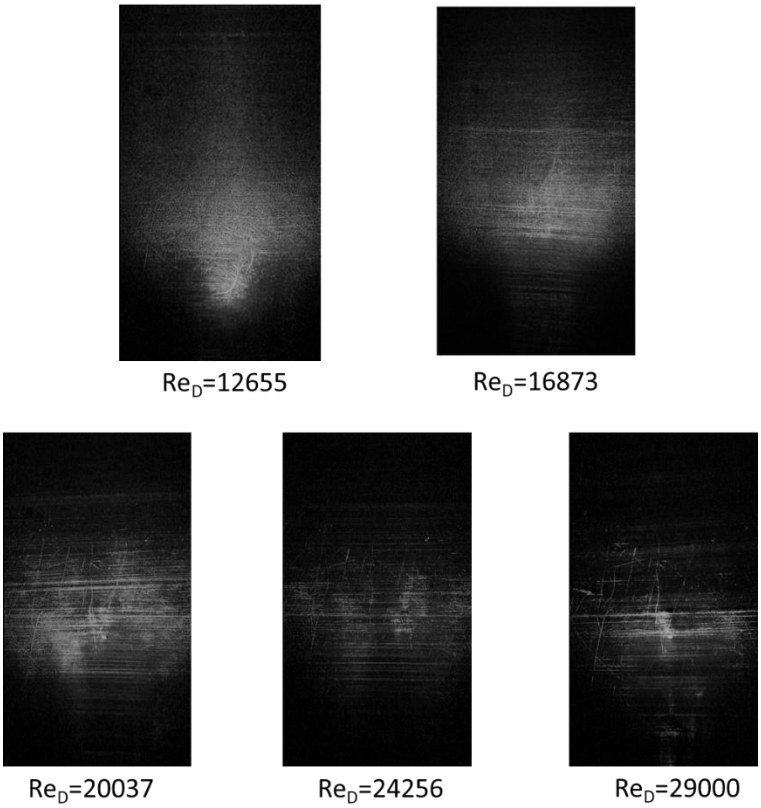

Figure 39: Dust deposition patterns for G/D=0.2

A similar result was also obtained at the case of G/D=0.2. Main dust settling down area seem to spread to the same region. However, this time dust concentration in spanwise direction is more concentrated along the center line when it is compared to G/D=0.1 case.

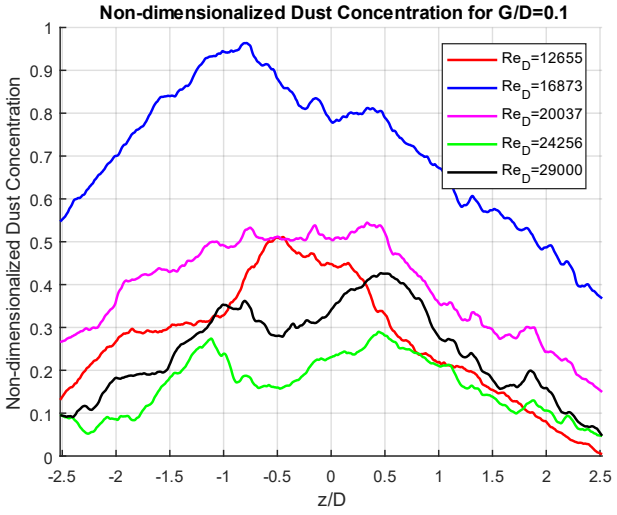

(a)

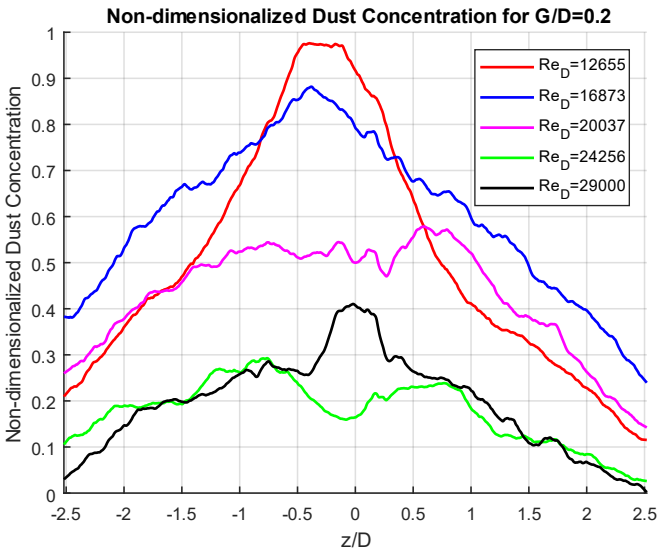

(b)

Figure 40: Dust concentration in spanwise direction
(a) G/D=0.1 and (b) G/D=0.2

More dust concentration, depending on increasing gap height, around the center line of wind tunnel implies that gap flow has more momentum to carry particles without letting them gain velocity in the spanwise direction. This situation can also be seen for the higher value of gap to diameter ratio.

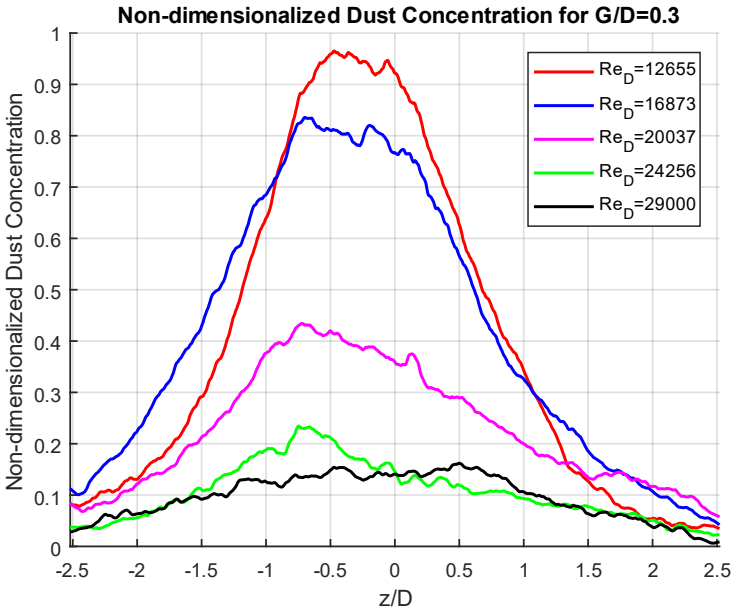

(a)

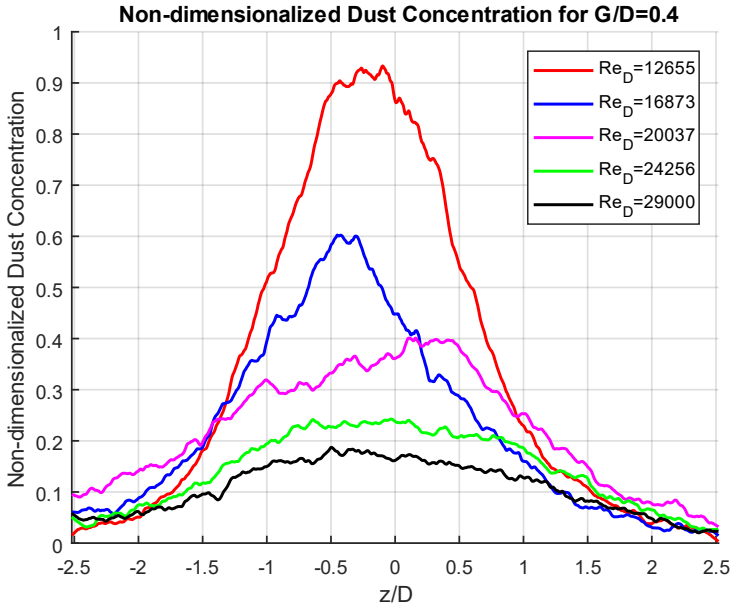

(b)

Figure 41: Dust concentration in spanwise direction
(a) G/D=0.3 and (b) G/D=0.4

When we go back to streamwise dust concentration distribution, besides G/D=0.1 and G/D=0.2, for the cases at G/D=0.3 dust deposition areas, seem to cover a location independent from Reynolds number.

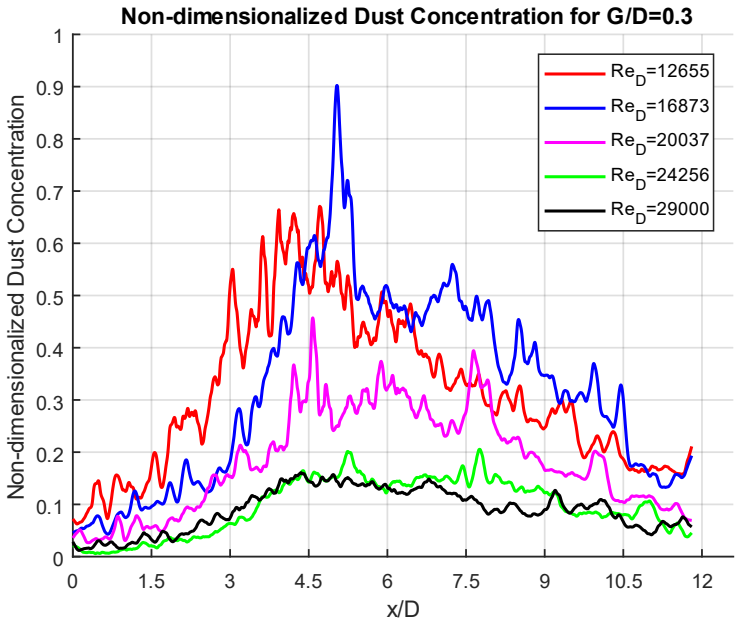

Figure 42: Dust concentration in streamwise direction for G/D=0.3

On the other hand, it is not a possibility to make a strong implication for higher cylinder heights about the relationship between cylinder height and Reynolds number, because either air velocity is not sufficient to lift particles or gap flow is too high to let particles settle down. Because of these reasons, just a trace amount of dust particle settles down, and it does not allow us to say anything meaningful along the streamwise direction.

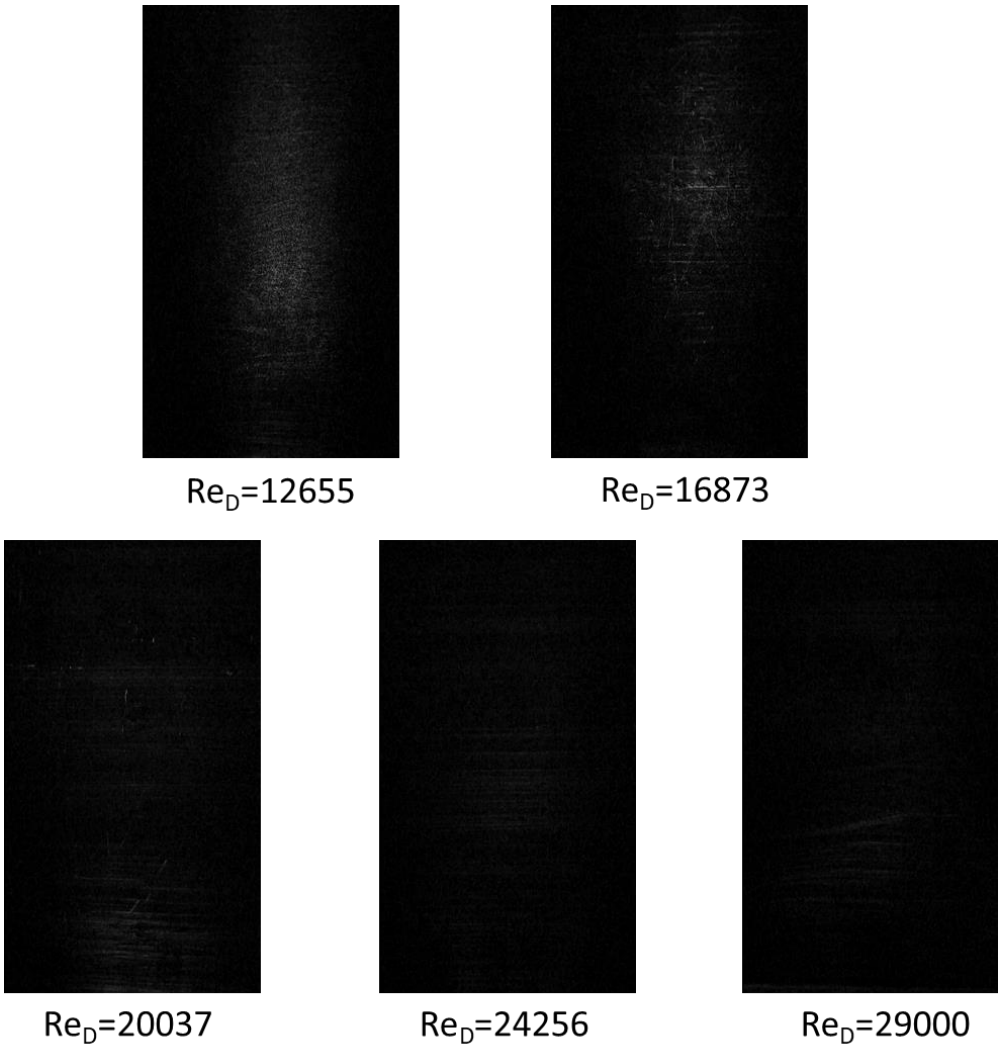

Figure 43: Dust deposition patterns for G/D=0.4

Chapter 6

Conclusions and Future Works

In this study, dust dispersion and dust deposition experiments were conducted in a wind tunnel, to observe the effects of free stream velocity and the gap between cylinder and wall on dispersion and deposition of dust particles. Results show remarkable similarities to previous cylinder wake studies which were conducted as single-phase flow, due to most probably Stokes numbers of the particle are between 2.5 and 5.5, it is a situation that allows the particle to be entrained by vortices and flung beyond the fluid mixing region.

Dust particles velocity fields depict that smaller gap between wall and cylinder results as closer recirculation area for dust particles, increasing gap moves away recirculation area from the cylinder in the streamwise direction. Furthermore, dust particle velocity fields show similarity to single phase velocity fields.

Results demonstrate that there is a critical number for the gap to diameter ratio, which is around 0.3 and it is a similar value to previous works. Although particles can find more chance spread in the spanwise direction below this critical number, they act like jet shooting above that critical value, and they concentrate around the center line. Furthermore, the amount of particles, that disperse and settle down is sharply changing below and above this critical number. In very small gap to diameter ratio, dust particles settle down is observed immediately after cylinder due to weakened gap flow.

The most exciting result is dust settle down locations seem independent from Reynolds number, results show dust deposition area, especially in the streamwise direction, changes by the gap to diameter ratio.

Although this study focuses only effects of Reynolds number and gap between cylinder and wall, there are many other contributing parameters such as humidity, temperature, the chemical mixture of dust particles and particle size, to dust dispersion and deposition, as mentioned in literature review section. Those factors require further experimental and analytical works to a better understanding of this phenomena. On the other hand, the effect of spinning tire and exhaust heat on dust dispersion behind a moving vehicle were neglected in this work, and they stand as potential investigation topic for the future.

References

[1] B. Kempinski and C. Murphy, “Technical challenges of the us army’s ground combat vehicle program,” DTIC Document, 2012.

[2] H. A. Nasrallah and R. C. Balling, “Impact of desertification on temperature trends in the middle east,” *Environmental Monitoring and Assessment*, vol. 37, no. 1, pp. 265–271, 1995.

[3] W. Humphries and J. Vincent, “The transport of airborne dusts in the near wakes of bluff bodies,” *Chemical Engineering Science*, vol. 33, no. 8, pp. 1141–1146, 1978.

[4] H. Choi, J. Lee, and H. Park, “Aerodynamics of heavy vehicles,” *Annual Review of Fluid Mechanics*, vol. 46, pp. 441–468, 2014.

[5] M. Carpentieri, P. Kumar, and A. Robins, “An overview of experimental results and dispersion modelling of nanoparticles in the wake of moving vehicles,” *Environmental Pollution*, vol. 159, pp. 685–693, 2010.

[6] J. Cimbala, H. Nagib, and A. Roshko, “Large structure in the far wakes of two-dimensional bluff bodies,” *Journal of Fluid Mechanics*, vol. 190, pp. 265-298, 1988.

[7] C. J. Baker, “Flow and dispersion in ground vehicle wakes,” *Journal of Fluids and Structures*, vol. 15, no. 7, pp. 1031-1060, 2001.

[8] M. Hanlon, *Bugatti Veyron 16.4 enters production.* Retrieved from https://newatlas.com/go/4808/ [Accessed 27 September 2018].

[9] V. Etyemezian, J. Gillies, H. Kuhns, D. Nikolic, J. Watson, J. Veranth, R. Labban, G. Seshadri, and D. Gillett, “Field Testing and Evaluation of Dust Deposition and Removal Mechanisms: Final Report,” Report Prepared for WESTAR Council, Lake Oswego, OR, by DRI: Las Vegas, NV, 2003.

[10] eSchoolToday, [Online]. Available: http://www.eschooltoday.com/landforms/the-process-of-wind-erosion.html [Accessed 27 September 2018].

[11] D. Goossens and B. Buck, “Dynamics of dust clouds produced by off-road vehicle driving,” *Journal of Earth Sciences and Geotechnical Engineering*, vol. 4, no. 2, pp. 1-21, 2014.

[12] J. M. Veranth, E. R. Pardyjak, and G. Seshadri, "Vehicle-generated fugitive dust transport: analytic models and field study," *Atmospheric Environment*, vol. 37, no. 16, pp. 2295–2303, 2003.

[13] R. Neulicht, J. Shular, *Emission Factor Documentation for AP-42 Section 13.2.2 Unpaved Roads Final Report*, U. S. Environmental Protection Agency, Research Triangle Park, NC, 1998.

[14] R. I. Dyck and J. J. Stukel, "Fugitive dust emissions from trucks on unpaved roads," *Environmental Science & Technology*, vol. 10, no. 10, pp. 1046–1048, 1976.

[15] U. S. Environmental Protection Agency, "Particulate Matter (PM) Pollution." [Online]. Available: https://www.epa.gov/pm-pollution [Accessed August 2018].

[16] B. Chakradhar, "Fugitive dust emissions from mining areas," *Journal of Environmental Systems*, vol. 31, no. 3, pp. 279–288, 2004.

[17] J. Gillies, V. Etyemezian, H. Kuhns, D. Nikolic, and D. Gillette, "Effect of vehicle characteristics on unpaved road dust emissions," *Atmospheric Environment*, vol. 39, no. 13, pp. 2341–2347, 2005.

[18] K. W. Nicholson, J. R. Branson, P. Giess, and R. J. Cannell, "The effects of vehicle activity on particle resuspension," *Journal of Aerosol Science*, vol. 20, no. 8, pp. 1425-1428, 1989.

[19] J. Watson, J. Chow, J. Gillies, H. Moosmuller, C. Rogers, D. DuBois, and J. Derby, "Effectiveness demonstration of fugitive dust control methods for public unpaved roads and unpaved shoulders on paved roads," *DRI Document No*, pp. 685–5200, 1996.

[20] L. R. Anspaugh, J. H. Shinn, P. L. Phelps, and N. C. Kennedy, "Resuspension and Redistribution of Plutonium in Soils," *Health Physics*, vol. 29, no. 4, pp. 571-587, 1975.

[21] J. F. Kok, E. J.R. Parteli, T.I. Michaels, and D. B. Karam, "The physics of wind-blown sand and dust," *Reports on Progress in Physics*, vol. 75, 2012.

[22] J. Wieringa, "Representative roughness parameters for homogeneous terrain," *Boundary Layer Meteorology*, vol. 63, pp. 323-363, 1993.

[23] D. Schulze, *Powders and bulk solids; behavior, characterization and flow*, Springer-Verlag Berlin Heidelberg, 2008.

[24] S. C. Alfaro, "Influence of soil texture on the binding energies of fine mineral dust particles potentially released by wind erosion," *Geomorphology*, vol. 93, no. 3-4, pp. 157-167, 2008.

[25] N. L. Klocke, and G. W. Hergert, "G90-964 How Soil Holds Water," Historical Materials from University of Nebraska Lincoln Extension, 1990. [Online]. Available: http://digitalcommons.unl.edu/extensionhist/725/ [Accessed August 2018]

[26] M. Darwish, *Threshold Friction Velocity: Moisture and Particle Size Effects* (Master's Thesis), Texas Tech University, Lubbock, Texas, 1991.

[27] R. A. Bagnold, *The physics of blown sand and desert dunes*, SAGE Publications Ltd, 1941.

[28] J. Li, T. Kandakji, J. A. Lee, J, Tatarko, J. Blackwell III, T. E. Gill, and J. D. Collins, "Blowing dust and highway safety in the southwestern United States: Characteristics of dust emission "hotspots" and management implications," *Science of Total Environment*, vol. 621, pp. 1023-103, 2018.

[29] B. Marticorena, and G. Bergametti, "Modeling the atmospheric dust cycle: 1. Design of a soil-derived dust emission scheme," *Journal of Geophysical Research*, vol. 100, no. D8, pp. 16415-16430, 1995.

[30] Z. Dong, Q. Mu, and X. Liu, "Defining the threshold wind velocity for moistened sediments," *Journal of Geophysical Research*, vol. 112, no. B8, p. B08202, 2007.

[31] J. Lelouvetel, F. Bigillon, D. Doppler, I. Vinkovic, J.Y. Champagne, "Experimental investigation of ejections and sweeps involved in particle suspension," *Water Resources Research*, vol. 45, 2009.

[32] J. Li, and K. Osada, "Preferential settling of elongated mineral dust particles in the atmosphere," *Geophysical Research Letters*, vol. 34, p. L17807,2007.

[33] W. C. Hinds, *Aerosol Technology: Properties, Behavior, and Measurement of Airborne Particles*, John Wiley & Sons, 1982.

[34] W. S. Chepil, "Influence of moisture on erodibility of soil by wind," *Soil Science Society of America Proceedings*, vol. 20, pp. 288-292, 1956.

[35] W. S. Chepil, "Properties of soil which influence wind erosion: I. The governing principle of surface roughness," *Soil Science Society of America Proceedings*, vol. 69, no.2, pp.149-162, 1950.

[36] W. B. Haines, "Studies in the physical properties of soils: II. A note on the cohesion developed by capillary forces in an ideal soil," *The Journal of Agricultural Science*, vol. 15, no. 4, pp. 529-535, 1925.

[37] J. A. Gillies, J. G. Watson, C. F. Rogers, D. DuBois, J. C. Chow, R. Langston, and J. Sweet, "Long-term efficiencies of dust suppressants to reduce PM_{10} emissions

from unpaved roads," *Journal of the Air & Waste Management Association*, vol. 49, no. 1, pp. 3-16, 1999.

[38] International Energy Agency, *World Energy Outlook 2007 China and India Insight*, OECD/IEA, 2007.

[39] P. Gillieron, and A. Kourta, "Aerodynamic drag reduction by vertical splitter plates," *Experiments in Fluids*, vol. 48, pp. 1-16, 2008.

[40] J. D. Kee, J. H. Rho, K. H. Kim, and D. H. Lee, "High speed driving stability of passenger car under crosswind effects," *International Journal of Automotive Technology*, vol. 15, no. 5, pp. 741−747, 2014.

[41] M. Arie, and H. Rouse, "Experiments on two-dimensional flow over a normal wall" *Journal of Fluid Mechanics*, vol. 1, no. 2, pp. 129-141, 1956.

[42] J. Y. Hwang, K. S. Yang, and S. H. Sun, "Reduction of flow-induced forces on a circular cylinder using a detached splitter plate," *Physics of Fluids*, vol. 15, no. 8, pp. 2433-2436, 2003.

[43] A.Mariotti, G.Buresti, and M.V.Salvetti, "Connection between base drag, separating boundary layer characteristics and wake mean recirculation length of an axisymmetric blunt-based body," *Journal of Fluids and Structures*, vol. 55, pp. 191-203, 2015.

[44] A. Mariotti, G. Buresti, G. Gaggini, and M. V. Salvetti, "Separation control and drag reduction for boat-tailed axisymmetric bodies through contoured transverse grooves," *Journal of Fluid Mechanics*, vol. 832, pp. 514-549, 2017.

[45] V. Durgesh, J. W. Naughton, and S. A. Whitmore, "Experimental Investigation of Base-Drag Reduction via Boundary-Layer Modification," *AIAA Journal*, vol. 51, no. 2, pp. 416-425, 2013.

[46] F. Gérardin, C. Gentric, and N. Midoux, "Particle dispersion in the near-wake of an isolated rotating wheel: Experimental and CFD study," *Journal of Aerosol Science*, vol. 76, pp. 56-71, 2014.

[47] P. A. Vaillancourt, and M. K. Yau, "Review of particle-turbulence interactions and consequences for cloud physics," *Bulletin of the American Meteorological Society*, vol. 85, no. 2, pp. 285-298, 2000.

[48] J. P. Minier, and E. Peirano, "The pdf approach to turbulent polydispersed two-phase flows," *Physics Report*, vol. 352, pp. 1-214, 2001.

[49] F. Mashayek and R. Pandya, "Analytical description of particle/droplet-laden turbulent flows," *Progress in Energy and Combustion Science*, vol. 29, no. 4, pp. 329–378, 2003.

[50] S. Sundaram, and L. R. Collins, "Numerical considerations in simulating a turbulent suspension of finite-volume particles," *Journal of Computational Physics*, vol. 124, pp. 337-350, 1996.

[51] Q. Chen, and G. Ahmadi, "Deposition of particles in a turbulent pipe flow," *Journal of Aerosol Science*, vol. 28, no. 5, pp. 789-769, 1997.

[52] Y. Tsuji, "Activities in discrete particle simulation in Japan," *Powder Technology*, vol. 113, pp. 278-286, 2000.

[53] K. Kiger, "https://enme.umd.edu/research/fluid-dynamics," University of Maryland Mechanical Engineering. [Online]. Available: https://www2.cscamm.umd.edu/programs/trb10/presentations/Multiphase_Turbulent_Flow.pdf [Accessed September 2018].

[54] B.Vreman, B. J. Geurts, N. G. Deen, J. A. M. Kuipers, and J. G. M. Kuerten, "Two- and four-way coupled Euler–Lagrangian large-eddy simulation of turbulent particle-laden channel flow," *Flow, Turbulence and Combustion*, vol. 82, pp. 47-71, 2009.

[55] S. Lain, "Study of turbulent two-phase gas-solid flow in horizontal channels," *Indian Journal of Chemical Technology*, vol. 20, pp. 128-136, 2013.

[56] T. Strömgren, "Modelling of turbulent gas-particle flow," Technical Reports from Royal Institute of Technology Department of Mechanics SE-100 44 Stockholm, Sweden, 2008.

[57] P. Traoré, J. C. Laurentie, and L. Dascalescu, "An efficient 4 way coupling CFD–DEM model for dense gas–solid particulate flows simulations," *Computers & Fluids*, vol. 113, pp. 65-76, 2015.

[58] G. A. Kallio, and M. W. Reeks, "A numerical simulation of particle deposition in turbulent boundary layers," *International Journal of Multiphase Flow*, vol. 15, no. 3, pp. 433-446, 1989.

[59] B. Oestrele, "On heavy particle dispersion in turbulent shear flows: 3-D analysis of the effects of crossing trajectories," *Boundary-Layer Meteorology*, vol. 130, pp. 71-95, 2009.

[60] M. Reeks, "On the dispersion of small particles suspended in an isotropic turbulent fluid," *Journal of Fluid Mechanics*, vol. 83, no. 3, pp. 529–546, 1977.

[61] M. R. Maxey, "The gravitational settling of aerosol particles in homogeneous turbulence and random flow fields," *Journal of Fluid Mechanics*, vol. 174, pp. 441–465, 1987.

[62] L. P. Wang, and M. R. Maxey, “Settling velocity and concentration distribution of heavy particles in homogeneous isotropic turbulence,” *Journal of Fluid Mechanics,* vol. 256, pp. 27-68, 1993.

[63] A. Berlemont, P. Desjonqueres, and G. Gouesbet, “Particle Lagrangian simulation in turbulent flows,” *International Journal of Multiphase Flow,* vol. 16, no. 1, pp. 19-34, 1990.

[64] G. I. Taylor, “Statistical theory of turbulence,” *Proceedings of the Royal Society of London. Series A - Mathematical and Physical Sciences,* vol. 151, pp. 421-444, 1935.

[65] I. Arad, V. S. L’vov, and I. Procaccia, “Correlation functions in isotropic and anisotropic turbulence: The role of the symmetry group,” *Physical Review E,* vol. 59, no. 6, pp. 6753-6765, 1999.

[66] N. Raju, and E. Meiburg, “The accumulation and dispersion of heavy particles in forced two-dimensional mixing layers. Part 2: The effect of gravity,” *Physics of Fluids,* vol. 7, no. 6, pp. 1241-1264, 1995.

[67] W. Uijttewaal, and R. Oliemans, “Particle dispersion and deposition in direct numerical and large eddy simulations of vertical pipe flows,” *Physics of Fluids,* vol. 8, no. 10, pp. 2590–2604, 1996.

[68] A. Nejat, V. Abdollahi, and K. Vahidkhah, “Lattice Boltzmann simulation of non-Newtonian flows past confined cylinders,” *Journal of Non-Newtonian Fluid Mechanics,* vol. 166, pp. 689-697, 2011.

[69] Y. Xia, J. Lin, and X. Ku, “Flow-induced rotation of circular cylinder in Poiseuille flow of power-law fluids,” *Journal of Non-Newtonian Fluid Mechanics,* vol. 260, pp. 120-132, 2018.

[70] R. Fitzpatrick, Boundary Layer Seperation, 22 January 2016. [Online]. Available: https://farside.ph.utexas.edu/teaching/336L/Fluid/node116.html [Accessed August 2018].

[71] J. B. Freund, J. G. Goetz, K. L. Hill, and J. Vermot, “Fluid flows and forces in development: Functions, features and biophysical principles,” *Development,* vol. 139, no. 7, pp.1129-1245, 2012.

[72] B.Weigand, and V. Simon, “Laws of similarity in fluid mechanics,” *Flow Phenomena in Nature,* vol. 1, pp. 20–35, 2006.

[73] D. Goossens, “The granulometrical characteristics of a slowly moving dust cloud,” *Earth Surface Process and Landforms,* vol. 10, pp. 353-362, 1985.

[74] F. Mashayek, and R. Pandya, "Analytical description of particle/droplet-laden turbulent flows," *Progress in Energy and Combustion Science*, vol. 29, no. 4, pp. 329–378, 2003.

[75] E. Loth, "Numerical approaches for motion of dispersed particles, droplets and bubbles," *Progress in Energy and Combustion Science*, vol. 26, pp. 161-223, 2000.

[76] S. Elghobashi, "On predicting particle-laden turbulent flows," *Applied Scientific Research*, vol. 52, pp. 309-329, 1994.

[77] A. W. Vreman, "Turbulence characteristics of particle-laden pipe flow," *Journal of Fluid Mechanics*, vol. 584, pp. 235-279, 2007.

[78] Y. Li, J. B. McLaughlin, K. Kontomaris, and L. Portela, "Numerical simulation of particle-laden turbulent channel flow," *Physics of Fluids*, vol. 13, no. 10, pp. 2957-2967, 2001.

[79] C. H. Moeng, "A large-eddy-simulation model for the study of planetary boundary-layer turbulence," *Journal of Atmospheric Sciences*, vol. 41, no. 13, pp. 2052-2062, 1984.

[80] M. W. Vance, K. D. Squires, and O. Simonin, "Properties of the particle velocity field in gas-solid turbulent channel flow," *Physics of Fluids*, vol. 18, no. 6, p. 063302, 2006.

[81] M. Ishii and T. Hibiki, *Thermo-fluid dynamics of two-phase flow*. Springer Science & Business Media, 2010.

[82] H.P. Zhu, Z.Y. Zhou, R.Y. Yang, and A.B. Yu, "Discrete particle simulation of particulate systems: Theoretical developments," *Chemical Engineering Science*, vol. 62, pp. 3378-3396, 2007.

[83] X. L. Tong, E. Luke, R. Smith, "Numerical validation of a near- field fugitive dust model for vehicles moving on unpaved surfaces," *Journal of Automobile Engineering*, vol. 228, no. 7, pp. 747-757, 2014.

[84] J. Berger, *Dispersion and Emission Modelling of Traffic Induced road Dust* (Doctoral Dissertation), University of Oslo, Oslo, Norway, 2010.

[85] A.G. Laptev, M.M. Basharov, T. M. Farakhov, A.R. Iskhakov, "Calculating Efficiency of Separation of Aerosol Particles from Gases in Packed Apparatuses," *Advances in Chemical Engineering and Science*, no. 4, pp. 143-148, 2014.

[86] X.K. Wang and S.K. Tan, "Near-wake flow characteristics of a circular cylinder close to a wall," *Journal of Fluids and Structures*, vol. 24(5), pp.605-627, 2008.

[87] P.W. Bearman, M.M. Zdravkovich, “Flow around a circular cylinder near a plane boundary,” *Journal of Fluid Mechanics,* no. 89, pp. 33–47, 1978.

[88] A.J. Grass, P.W.J. Raven, R.J. Stuart, J.A. Bray, “The influence of boundary layer velocity gradients and bed proximity on vortex shedding from free spanning pipelines,” *ASME Journal of Energy Resources Technology,* vol.106, pp. 70–78, 1984.

[89] S. Taniguchi, K. Miyakoshi, “Fluctuating fluid forces acting on a circular cylinder and interference with a plane wall,” *Experiments in Fluids,* vol. 9, pp. 197–204, 1990.

[90] G. Buresti, A. Lanciotti, “Mean and fluctuating forces on a circular cylinder in cross-flow near a plane surface,” *Journal of Wind Engineering and Industrial Aerodynamics*, vol. 41, pp. 639–650, 1992.

[91] J.-H. Choi, S.-J. Lee, “Ground effect of flow around an elliptic cylinder in a turbulent boundary layer,” *Journal of Fluids and Structures*, vol. 14, pp. 697–709, 2000.

[92] S.J. Price, D. Sumner, J.G. Smith, K. Leong, M.P. Paıdoussis, “Flow visualization around a circular cylinder near to a plane wall,” *Journal of Fluids and Structures,* vol. 16, pp. 175–191, 2002.

[93] G.S. He, J.J. Wang, C. Pan, L.H. Feng, Q. Gao, A. Rinoshika, “Vortex dynamics for flow over a circular cylinder in proximity to a wall,” *Journal of Fluid Mechanics,* vol. 812, pp. 698-720, 2017.

[94] C. Lei, L. Cheng, K. Kavanagh, “Re-examination of the effect of a plane boundary on force and vortex shedding of a circular cylinder,” *Journal of Wind Engineering and Industrial Aerodynamics*, vol. 80, pp. 263–286, 1999.